Effect of In Situ Grown BNNTs and Preparation Temperature on Mechanical Behavior of SiC/SiC Minicomposites

Shenwei Xu
Central South University
Huilong Pi
Northwestern Polytechnical University
Pengfei Wu
Central South University
Yuan Shi
German Aerospace Center DLR Institute of Planetary Research: Deutsches Zentrum fur Luft- und Raumfahrt DLR Institut fur Planetenforschung
Haitang Yang (hai.tang.ouyang@hotmail.com)
Central South University
Longbiao Li
Nanjing University of Aeronautics and Astronautics
Xiaozhong Huang
Central South University

Research Article

Keywords: Ceramic matrix composites (CMCs), Boron nitr ide nanotubes (BNNTs) BNNTs), M ech anical behavior, Precurs or Infiltration and Pyrolysis PIP

Posted Date: March 8th, 2021

DOI: https://doi.org/10.21203/rs.3.rs-284157/v1

Effect of In Situ Grown BNNTs and Preparation Temperature on Mechanical Behavior of SiC/SiC Minicomposites

Shenwei Xu[a, b, c,†], Huiling Pi[d,†], Pengfei Wu[e], Yuan Shi[f],

Haitang Yang[a,b,c,g*], Longbiao Li[h]

[a] *Powder Metallurgy Research Institute, Central South University, Changsha, Hunan 410083, China*

[b] *State Key Laboratory of Powder Metallurgy, Central South University, Changsha, Hunan 410083, China*

[c] *Hunan Province Key Laboratory of New Specialty Fibers and Composite Material, Central South University, Changsha, Hunan 410083, China*

[d] *Science and Technology on Thermostructural Composite Materials Laboratory, Northwestern Polytechnical University, Xi¢an, Shanxi 710072, China*

[e] *School of Aeronautics and Astronautics, Central South University, Changsha, Hunan 410083, China*

[f] *Institute of Structures and Design, German Aerospace Center Stuttgart, Pfaffenwaldring 38-40, 70569 Stuttgart, Germany*

[g] *State Key Laboratory of High Performance Complex Manufacturing, Central South University, Changsha, Hunan 410083, China*

[h] *College of Civil Aviation, Nanjing University of Aeronautics and Astronautics, No.29, Jiangjun Ave., Nanjing 211106, PR China*

† Shenwei Xu and Huiling Pi contributed equally to this work

* Corresponding author:

Email: hai.tang.ouyang@hotmail.com

Abstract

In this paper, effect of in situ grown boron nitride nanotubes (BNNTs) and preparation temperature on mechanical behavior of PIP (Precursor Infiltration and Pyrolysis) SiC/SiC minicomposites under monotonic and compliance tensile is investigated. In situ BNNTs are grown on the surface of SiC fibers using ball milling – annealing process. Composite elastic modulus, tensile strength, fracture strain, tangent modulus, and loading/unloading inverse tangent modulus (ITM) are obtained and adopted to characterize the mechanical properties of the composites. Microstructures of in situ grown BNNTs and tensile fracture surfaces are observed under scanning electronic microscopic (SEM). For SiC/SiC minicomposites with BNNTs, the elastic modulus, tensile strength, and fracture strain are all lower than those of SiC/SiC minicomposites without BNNTs, mainly due to high preparation temperature and the oxidation of the PyC interphase during the annealing process. Tensile stress-strain curves of SiC/SiC minicomposites with and without BNNTs are predicted using the developed micromechanical constitutive model. The predicted results agreed with experimental data. This work will provide guidance for predicting the service life of SiC_f/SiC composite materials and may enable these materials to become a backbone for thermal structure systems in aerospace applications.

Keywords: Ceramic-matrix composites (CMCs); Boron nitride nanotubes (BNNTs); Mechanical behavior; Precursor Infiltration and Pyrolysis (PIP).

1. Introduction

Continuous silicon carbide fiber reinforced silicon carbide ceramic matrix composites (SiC/SiC CMCs) have the advantages of low density, high temperature resistance, oxidation resistance, high specific strength, and high specific modulus, and have become an important candidate material for the hot-section components of next generation high-performance aero-engine [[1]-[4]]. The introduction of fiber and the design of fiber/matrix interface can stimulate the energy consumption mechanism such as interfacial debonding and crack deflection and endow the material with non-brittle fracture characteristics [[5]]. However, on the one hand, the matrix between fibers, between fiber bundles and between layers is brittle ceramics and difficult to be strengthened and toughened by the energy consumption mechanism in micron scale; on the other hand, the crack initiation threshold in the matrix is low, and the crack propagation cannot be hindered, which ultimately limits the mechanical properties of the material. Therefore, as the weak region in the material, the micro region of matrix needs to be strengthened and toughened in a finer scale to improve its properties. Boron nitride nanotubes (BNNTs) have excellent mechanical, chemical and thermal stability. The oxidation resistance temperature is up to 900 ^{o}C. The introduction of BNNTs into the material, as the second reinforcement in addition to the microfiber, can improve the mechanical properties of the matrix by strengthening and toughening the micro area matrix in the nano scale, and finally realize the optimization of the overall properties of the material [[6]-[8]].

Many researchers performed experimental and theoretical investigations on the mechanical behavior of ceramic or CMCs with BNNTs. Bansal et al. [[9], [10]] firstly introduced BNNTs into ceramic materials to prepare BNNTs reinforced barium calcium aluminosilicate (BACS) glass. Experimental results showed that the room temperature bending strength and fracture toughness of the glass increased by 90% and 35% respectively after adding 4 wt% BNNTs, which verified the strengthening and toughening effect of BNNTs. Based on the experimental results, Bansal et al [[9], [10]]

analyzed that the debonding and pull-out mechanism of BNNTs is similar to the strengthening and toughening mechanism of fiber or whisker, which may be the reason for the improvement of glass strength and toughness. Huang et al. [[11]] studied the BNNTs reinforced Al_2O_3 and Si_3N_4 composites. The results showed that the Vickers hardness of Al_2O_3 increased from 17.3 to 19.1 GPa when the content of BNNTs increased to 0.5 wt%, and the hardness decreased to 14.5 GPa when the content of BNNTs increased to 2.5 wt%. The Young's modulus decreased with the content of BNNTs increased. The Vickers hardness and Young's modulus of Si_3N_4 decreased with the increase of BNNTs content. However, the high temperature plastic deformation ability of the two ceramics was greatly improved after the introduction of BNNTs. Hurst [[12]] verified the feasibility of in-situ growth of BNNTs in SiC fiber bundles and SiC fiber preforms and confirmed the strengthening effect of BNNTs on the mechanical properties of SiC/SiC composites. Using B powder, B_2O_3 powder, N_2 and NH_3 as raw materials, BNNTs were successfully grown on the surface and inside of fiber bundles and fiber preforms by CVD method. The introduction of BNNTs into the fibers of SiC/SiC composites can reduce the number of crack initiation in the matrix and eventually improve the tensile strength. The modeling of mechanical properties is a prerequisite for the further development and application of PIP SiC/SiC composite. Li et al. [[13], [14]] developed a micromechanical constitutive model to predict the monotonic and cyclic tensile behavior of unidirectional, cross-ply, and 2D plain-woven CMCs. Li [[15]] analyzed the effect of stochastic loading on tensile behavior of different CMCs. Li [[16]] developed a time-dependent tensile constitutive model to predict the tensile stress-strain curves considering time-dependent interface damage and fibers fracture. Up until now, it has not been studied the effects of the preparation temperature of BNNTs on the mechanical properties of SiC/SiC composites.

The objective of this paper is to fabricate the SiC/SiC minicomposites with and without BNNTs. The mechanical behavior of SiC/SiC with, without BNNTs and the preparation temperature is investigated under monotonic and compliance tensile loading. Microstructures of BNNTs are observed under the scanning electronic microscopic (SEM), and the tensile damage and fracture process are analyzed and related with micro

damage mechanisms insider of composites. A micromechanical constitutive relationship is developed to predict the nonlinear mechanical behavior of SiC/SiC minicomposites. The composite's tangent modulus and unloading and reloading inverse tangent modulus (ITM) are calculated and analyzed to characterize the tensile damage behavior of the composites. The composite's tensile strength, fracture strain, tangent modulus, loading/unloading ITMs are compared between SiC/SiC minicomposites with and without BNNTs.

2. Materials and experimental procedures

To develop the in situ BNNTs on the surface of SiC fiber, mixed powder of B powder, MgO powder and Fe_2O_3 powder with mass ratio of 2:1:1 was prepared. The precursor powder with uniform dispersion and smaller particle size was obtained by planetary ball mill milling for 100 h, and then spread evenly to the porcelain boat. The SiC fiber bundles with a PyC interface layer were wound on the porcelain boat covered with a layer of precursor powder, and then annealed in a tubular furnace at approximately 1300 ^{o}C, as shown in **Fig. 1**. In the early stage, Ar was used as the protective atmosphere. When the temperature was raised to approximately 1300 ^{o}C, NH_3 was used as the nitrogen source, and the annealing time was 120 min. After annealing, it is cooled down to room temperature. For comparison, the same SiC fiber bundles were wound on the porcelain boat without precursor powder and annealed accordingly. After the sample was taken out, it was found that the surface of fiber bundles with precursor powder in the porcelain boat became white, while the surface of fiber bundles without precursor powder had no obvious change. Then, the matrix of the two treated fiber bundles was densified by PIP process. Polycarbosilane (PCS) was used as raw material, and the weight gain was less than 1% after three PIP processes. **Table 1** listed the general properties of SiC/SiC mincomposites with and without BNNTs.

Table 1. General properties of SiC/SiC minicomposites

Type of sample	Porosity	Density	Fiber volume content	Fiber orientation
SiC/PyC/SiC	≤ 10 %	≤ 2.5 g/cm^3	45 %	Unidirectional

SiC/PyC/BNNTs/SiC	≤ 8 %	≤ 2.6 g/cm^3	45 %	Unidirectional

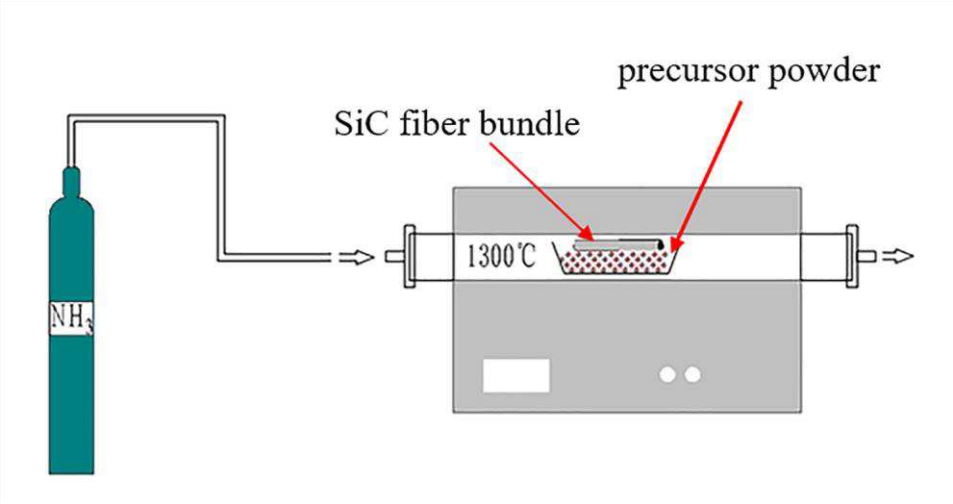

Fig. 1. Schematic of fabrication of BNNTs using ball milling – annealing method.

The fabricated SiC/SiC minicomposites with and without BNNTs were cut into the specimens with dimensions of 50 mm in total length, as shown in **Fig. 2**. Monotonic and cyclic compliance tensile tests were conducted on MTS Insight electrical tensile testing machine (MTS Systems Corp., Minneapolis, MN, USA), as shown in **Fig. 3**. Tensile tests were conducted under displacement control with the loading rate of 0.01 mm/min.

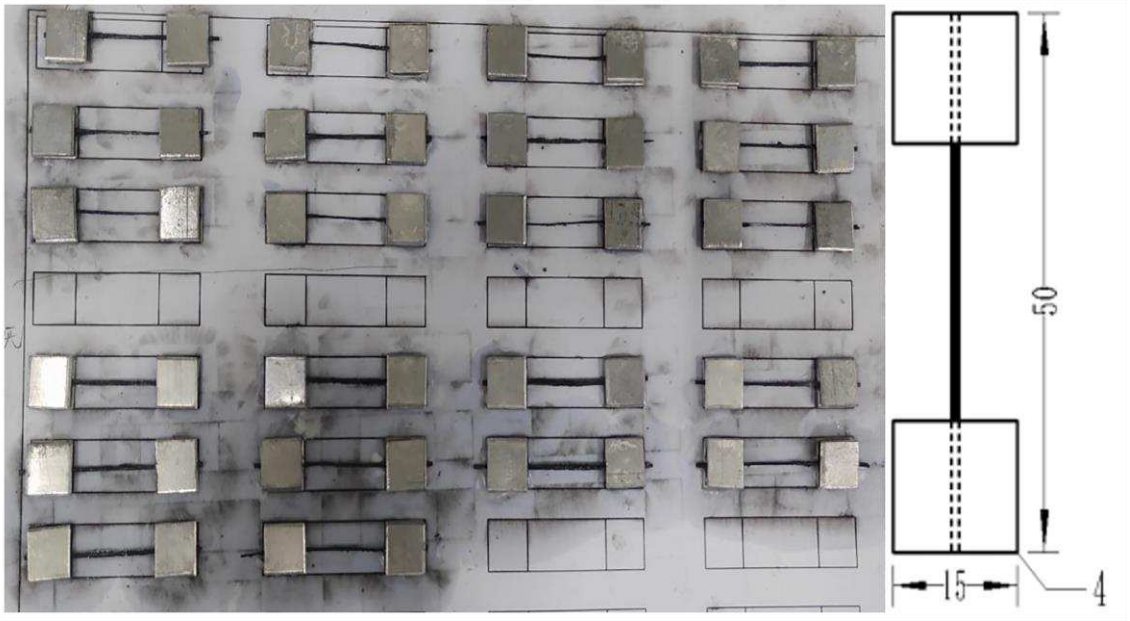

Fig. 2. Schematic of tensile specimens of SiC/SiC composites with and without BNNTs

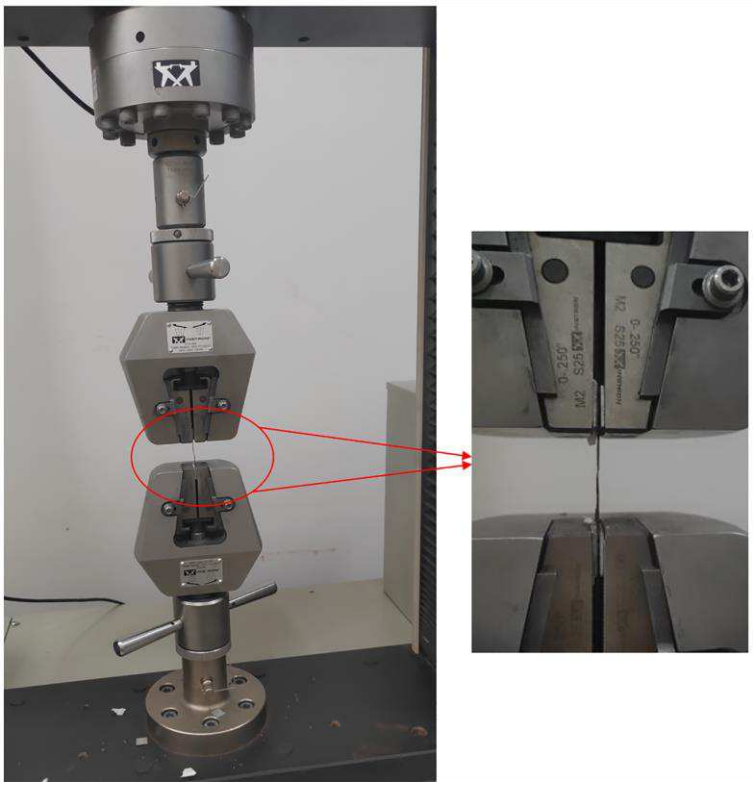

Fig. 3. Schematic of testing machine and tensile specimen.

3. Micromechanical constitutive model

Nonlinear behavior of mini-CMCs under tensile loading is mainly attributed to multiple micro damage mechanisms in the fiber, the matrix, and the interface between the fiber and the matrix [[16]-[18]]. Tensile nonlinear behavior of mini-CMCs can be divided into three main stages based on the internal damage state, including:

- Stage I, the linear-elastic region.
- Stage II, the nonlinear region due to micro damages.
- Stage III, the secondary linear and final fracture region due to gradual fiber fracture.

In this section, a micromechanical constitutive relationship of the three stages mentioned above is developed and related with micro damage state inside of mini-CMCs.

3.1. Stage

In Stage I, there is no damages occurred in mini-CMCs, and the linear-elastic stress-strain relationship is,

$$\varepsilon_{\mathrm{c}}=\frac{\sigma}{E_{\mathrm{c}}} \tag{1}$$

where σ is the applied stress, and E_{c} is the composite's elastic modulus.

3.2. Stage II

When multiple micro damage mechanisms occur in the mini-CMCs, the nonlinear stress-strain relationship is,

$$\varepsilon_{\mathrm{c}}(\sigma)=\begin{cases}\dfrac{\sigma}{V_{\mathrm{f}}E_{\mathrm{f}}}\eta-\dfrac{\tau_{\mathrm{i}}}{E_{\mathrm{f}}}\dfrac{l_{\mathrm{d}}}{r_{\mathrm{f}}}\eta+\dfrac{\sigma_{\mathrm{fo}}}{E_{\mathrm{f}}}(1-\eta)-\dfrac{1}{\rho E_{\mathrm{f}}}\dfrac{2r_{\mathrm{f}}}{l_{\mathrm{c}}}\left(\dfrac{V_{\mathrm{m}}}{V_{\mathrm{f}}}\sigma_{\mathrm{mo}}-2\dfrac{l_{\mathrm{d}}}{r_{\mathrm{f}}}\tau_{\mathrm{i}}\right) \\ \qquad\qquad\times\left[\exp\left(-\dfrac{\rho}{2}\dfrac{l_{\mathrm{c}}}{r_{\mathrm{f}}}(1-\eta)\right)-1\right]-(\alpha_{\mathrm{c}}-\alpha_{\mathrm{f}})\Delta\mathrm{T},\eta<1 \\ \dfrac{\sigma}{V_{\mathrm{f}}E_{\mathrm{f}}}-\dfrac{\tau_{\mathrm{i}}}{2E_{\mathrm{f}}}\dfrac{l_{\mathrm{c}}}{r_{\mathrm{f}}}-(\alpha_{\mathrm{c}}-\alpha_{\mathrm{f}})\Delta\mathrm{T},\eta=1\end{cases} \tag{2}$$

where V_{f} and V_{m} are the volume of the fiber and the matrix, E_{f} is the modulus of the fiber, τ_{i} is the shear stress at the interface, r_{f} is the fiber radius, l_{d} and l_{c} are the length of the debonding and the space between the cracking in the matrix, α_{f} and α_{c} are the axial thermal expansional coefficient of the fiber and the composite, and ΔT is the temperature difference between testing and fabricated temperature. Curtin [[19]] developed a stochastic model to analysis matrix stochastic cracking inside of CMCs, and the relationship between matrix crack spacing and applied stress can be determined by Eq. (3). Gao et al. [[20]] developed a fracture mechanical approach to determine the interface debonding length when matrix crack propagates to the interface, and the relationship between the interface debonding length and the applied stress can be determined by Eq. (4).

$$l_{\mathrm{c}}=l_{\mathrm{sat}}\left\{1-\exp\left[-\left(\frac{\sigma_{\mathrm{m}}}{\sigma_{\mathrm{R}}}\right)^{m}\right]\right\}^{-1} \tag{3}$$

$$l_{\mathrm{d}}=\frac{r_{\mathrm{f}}}{2}\left(\frac{V_{\mathrm{m}}E_{\mathrm{m}}\sigma}{V_{\mathrm{f}}E_{\mathrm{c}}\tau_{\mathrm{i}}}-\frac{1}{\rho}\right)-\sqrt{\left(\frac{r_{\mathrm{f}}}{2\rho}\right)^{2}+\frac{r_{\mathrm{f}}V_{\mathrm{m}}E_{\mathrm{m}}E_{\mathrm{f}}}{E_{\mathrm{c}}\tau_{\mathrm{i}}^{2}}\zeta_{\mathrm{d}}} \tag{4}$$

where l_{sat} is the saturation length of matrix cracking, σ_{m} is the stress carried by the matrix, σ_{R} is the characteristic stress for cracking in the matrix, and ζ_{d} is the debonding energy at the interface.

During damage Stage II, a new damage parameter of interface debonding ratio is,

$$\eta = 2\frac{l_{\mathrm{d}}}{l_{\mathrm{c}}} \tag{5}$$

3.3. Stage III

Upon approaching saturation of the cracking in the matrix, fibers gradually fracture inside of the composite. Considering fiber's failure, the stress-strain relationship at the Stage III is,

$$\varepsilon_{\mathrm{c}}(\sigma) = \begin{cases} \dfrac{\Phi}{E_{\mathrm{f}}}\eta - \dfrac{\tau_{\mathrm{i}}}{E_{\mathrm{f}}}\dfrac{l_{\mathrm{d}}}{r_{\mathrm{f}}}\eta + \dfrac{\sigma_{\mathrm{fo}}}{E_{\mathrm{f}}}(1-\eta) - \dfrac{1}{\rho E_{\mathrm{f}}}\dfrac{2r_{\mathrm{f}}}{l_{\mathrm{c}}}\left(\Phi - \sigma_{\mathrm{fo}} - 2\dfrac{l_{\mathrm{d}}}{r_{\mathrm{f}}}\tau_{\mathrm{i}}\right) \\ \qquad \times\left[\exp\left(-\dfrac{\rho}{2}\dfrac{l_{\mathrm{c}}}{r_{\mathrm{f}}}(1-\eta)\right) - 1\right] - (\alpha_{\mathrm{c}} - \alpha_{\mathrm{f}})\Delta\mathrm{T}, \eta < 1 \\ \dfrac{\Phi}{E_{\mathrm{f}}} - \dfrac{\tau_{\mathrm{i}}}{E_{\mathrm{f}}}\dfrac{l_{\mathrm{c}}}{2r_{\mathrm{f}}} - (\alpha_{\mathrm{c}} - \alpha_{\mathrm{f}})\Delta\mathrm{T}, \eta = 1 \end{cases} \tag{6}$$

where Φ is the intact fiber stress. The Global Load Sharing (GLS) criterion is adopted to determine the stress distribution between the intact and failure fibers [[21]]

$$\frac{\sigma}{V_{\mathrm{f}}} = \Phi(1-P) + \frac{2\tau_{\mathrm{i}}}{r_{\mathrm{f}}}\langle L\rangle P \tag{7}$$

where <*L*> is the average fiber pullout length, *P* is the fiber's failure probability.

$$P = 1 - \exp\left[-\left(\frac{\Phi}{\sigma_{\mathrm{fc}}}\right)^{m_{\mathrm{f}}+1}\right] \tag{8}$$

where σ_{fc} is the fiber characteristic strength, and m_{f} is the fiber Weibull modulus.

4. Results and discussions

In this section, experimental monotonic and compliance tensile behavior of SiC/SiC minicomposites with and without BNNTs are conducted. The mechanical properties of composite's Young's modulus, fracture strength, and failure strain are obtained. The cyclic loading/unloading inverse tangent modulus (ITM) corresponding to different tensile peak stresses are analyzed. The fracture surfaces of the SiC/SiC minicomposites with and without BNNTs are analyzed under SEM. Using the developed micromechanical constitutive model, the tensile properties of the SiC/SiC minicomposites with and without BNNTs are also predicted.

4.1 Monitonic and cyclic loading/unloading tensile of SiC/SiC minicomposites with and without BNNTs

Fig. 4 shows the monotonic tensile stress-strain curves of SiC/SiC minicomposite with and without BNNTs. Tensile stress-strain curves exhibited obvious nonlinear mechanical behavior due to the internal damage evolution. **Table 2 and 3** listed the tensile mechanical properties of SiC/SiC minicomposites with and without BNNTs.

- For SiC/SiC minicomposite with BNNTs, four specimens were tensile tested to fracture, and the composite's tensile elastic modulus was E_c = 71, 70.2, 71.5, and 83.5 GPa, respectively, the composite's tensile strength was σ_{UTS} = 262.8, 258.3, 253.5, and 268.1 MPa, respectively, and the corresponding fracture strain was ε_f = 0.374, 0.366, 0.383, and 0.366%, respectively. The average composite elastic modulus was approximately E_c = 74 GPa with the standard deviation of 5.47 GPa. The average tensile strength was approximately σ_{UTS} = 260.6 MPa with the standard deviation of 5.4 MPa. The average composite tensile fracture strain was approximately ε_f = 0.372% with the standard deviation of 0.007%.
- For SiC/SiC minicomposites without BNNTs, four specimens were tensile tested to fracture, and the composite's tensile elastic modulus was E_c = 90.2, 92.4, 95.9, and 92.1 GPa, respectively, the composite's tensile strength was σ_{UTS} = 485.6, 502.6, 482.9, and 507.8 MPa, respectively, and the corresponding tensile fracture strain was ε_f = 0.658, 0.683, 0.642, 0.648%, respectively. The average composite's elastic modulus was approximately E_c = 92.6 GPa with the standard deviation of 2 GPa. The average composite's tensile strength was approximately σ_{UTS} = 494.7 MPa with the standard deviation of 10.7 MPa. The average composite's tensile fracture strain was approximately ε_f = 0.657% with the standard deviation of 0.015%.

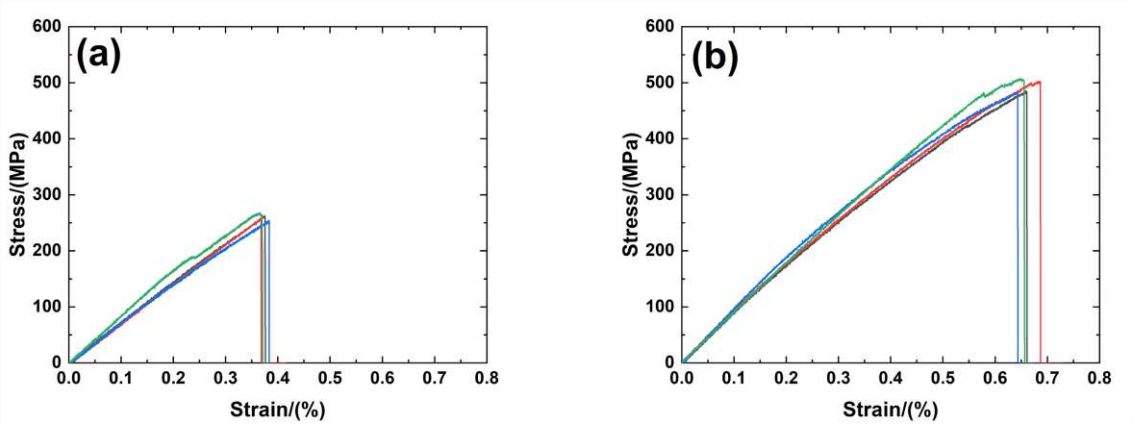

Fig. 4. Monotonic tensile stress-strain curves of SiC/SiC minicomposites (a) with BNNTs; and (b) without BNNTs

Table 2. Monotonic tensile properties of SiC/SiC minicomposites with BNNTs

Specimen	Elastic modulus/(GPa)	Tensile strength/(MPa)	Fracture strain/(%)
#1	71	262.8	0.374
#2	70.2	258.3	0.366
#3	71.5	253.5	0.383
#4	83.5	268.1	0.366
Average value	74	260.6	0.372
Standard deviation	5.47	5.4	0.007

Table 3. Monotonic tensile properties of SiC/SiC minicomposites without BNNTs

Specimen	Elastic modulus/(GPa)	Tensile strength/(MPa)	Fracture strain/(%)
#1	90.2	485.6	0.658
#2	92.4	502.6	0.683
#3	95.9	482.9	0.642
#4	92.1	507.8	0.648
Average value	92.6	494.7	0.657
Standard deviation	2	10.7	0.015

It can be found that the composite's elastic modulus, tensile strength, and fracture strain of SiC/SiC minicomposites with BNNTs are all less than those of SiC/SiC minicomposites without BNNTs. The degradation of the mechanical properties of SiC/SiC minicomposites with BNNTs is mainly attributed to the annealing at 1300 ^{o}C. In order to show the effect of annealing at 1300 ^{o}C on composite's mechanical properties. The SiC/SiC composite without BNNTs were also heat-treated at 1300 ^{o}C.

Fig. 5 shows the typical tensile stress-strain curve. The composite's tensile strength was approximately σ_{UTS} = 163 MPa, and the corresponding fracture strain was approximately ε_f = 0.31%. It can be found that after heat-treatment at 1300 °C, the mechanical properties of the SiC/SiC minicomposite degraded rapidly and were less than the values of SiC/SiC minicomposite with BNNTs.

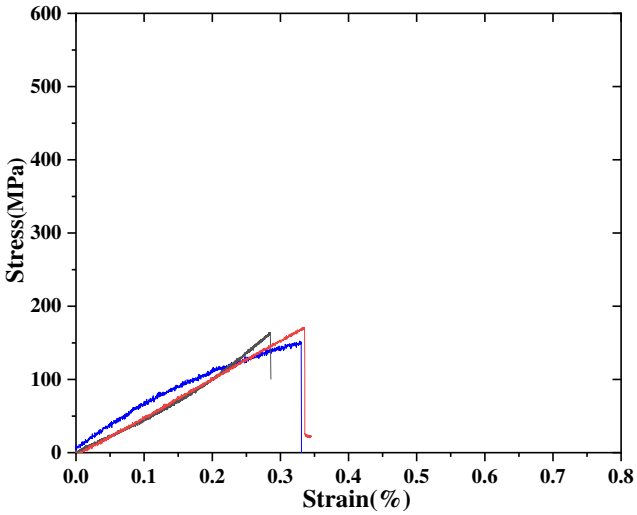

Fig. 5. Tensile stress-strain curve of SiC/SiC minicomposite after heat-treatment at 1300 °C

.

Fig. 6 shows the compliance tensile behavior of SiC/SiC minicomposite with and without BNNTs. Three specimens were conducted to the cyclic loading/unloading tests. For SiC/SiC with BNNTs, under tensile loading, the specimen was unloading at the peak stresses of σ_{max} = 75, 125, and 175 MPa to the valley stress of σ_{min} = 20 MPa, respectively, and then loading to final fracture. For SiC/SiC without BNNTs, under tensile loading, the specimen was unloading at different peak stresses of σ_{max} = 150, 250, and 350 MPa to the valley stress of σ_{min} = 20 MPa, and then tensile to final fracture.

- For SiC/SiC minicomposite with BNNTs, the unloading and reloading hysteresis loops exhibited non-closure appearance at peak and valley stress, and there is almost no permanent strain. However, for SiC/SiC minicomposite without BNNTs, the unloading and reloading hysteresis loops exhibited closure at the valley stress and non-closure at the peak stress, and there is clear permanent strain [[22]].
- For SiC/SiC minicomposite with BNNTs, the peak strains at the peak stresses of σ_{max} = 75, 125, and 175 MPa were ε_c = 0.096, 0.158, and 0.225%, and the

composite tensile fracture occurred at the stress of σ_{UTS} = 288.7 MPa with the fracture strain of ε_f = 0.42%.

- For SiC/SiC minicomposite without BNNTs, the peak strains at the peak stresses of σ_{max} = 150, 250, and 350 MPa were ε_c = 0.199, 0.361, and 0.523%, and the composite tensile fracture occurred at the stress of σ_{UTS} = 524 MPa with the fracture strain of ε_f = 0.86%.

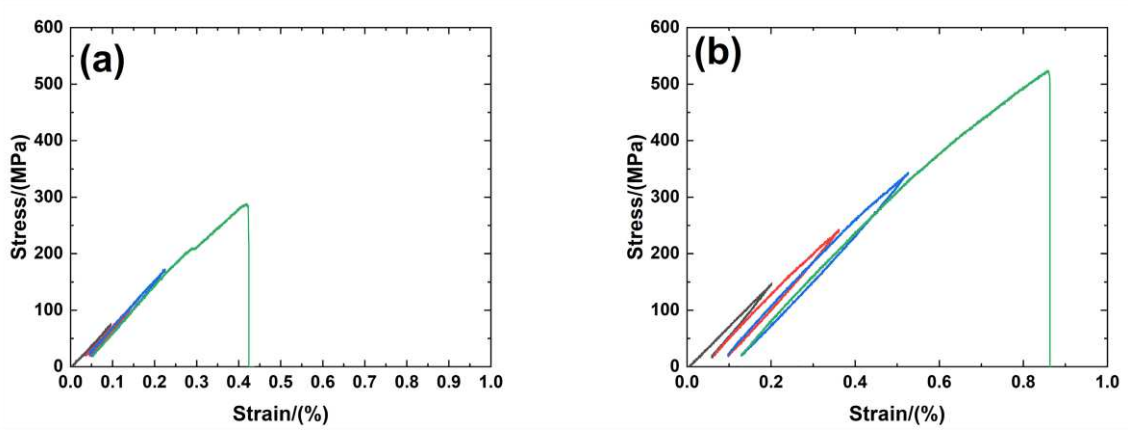

Fig. 6. Cyclic compliance tensile curves of SiC/SiC minicomposites (a) with BNNTs; and (b) without BNNTs

Fig.s 7 and 8 show the loading and unloading inverse tangent modulus (ITM) versus applied stress curves of SiC/SiC minicomposites with and without BNNTs.

- For SiC/SiC minicomposite with BNNTs, the loading ITM increased with increasing applied stress and then remained constant. However, when the peak stress increased from σ_{max} = 75 to 175 MPa, the constant ITM decreased from 12.6 TPa^{-1} to 12.1 TPa^{-1}. The unloading ITM increased with decreasing applied stress to the constant value. When the peak stress increased from σ_{max} = 75 to 175 MPa, the constant ITM increased from 10.8 TPa^{-1} to 11.2 TPa^{-1}.
- For SiC/SiC minicomposite without BNNTs, the loading ITM increased with increasing applied stress and then remained constant. However, when the peak stress increased from σ_{max} = 150 to 350 MPa, the constant ITM decreased from 13.6 TPa^{-1} to 13.2 TPa^{-1}. The unloading ITM increased with decreasing applied stress to the constant value. When the peak stress increased from σ_{max} = 150 to 350 MPa, the constant ITM increased from 10.8 TPa^{-1} to 12.3 TPa^{-1}.

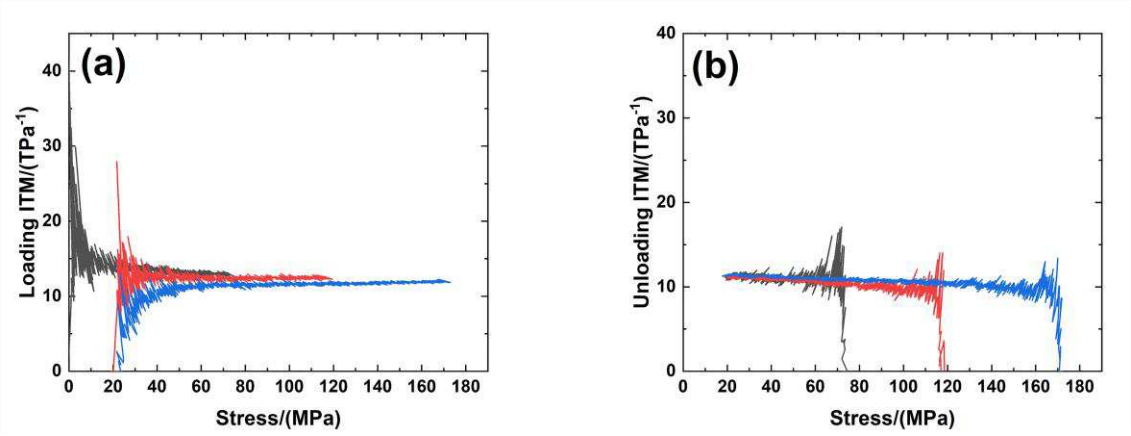

Fig. 7. (a) Loading ITM; and (b) unloading ITM versus applied stress curves of SiC/SiC minicomposite with BNNTs for different peak stresses of σ_{max} = 75, 125, and 175 MPa

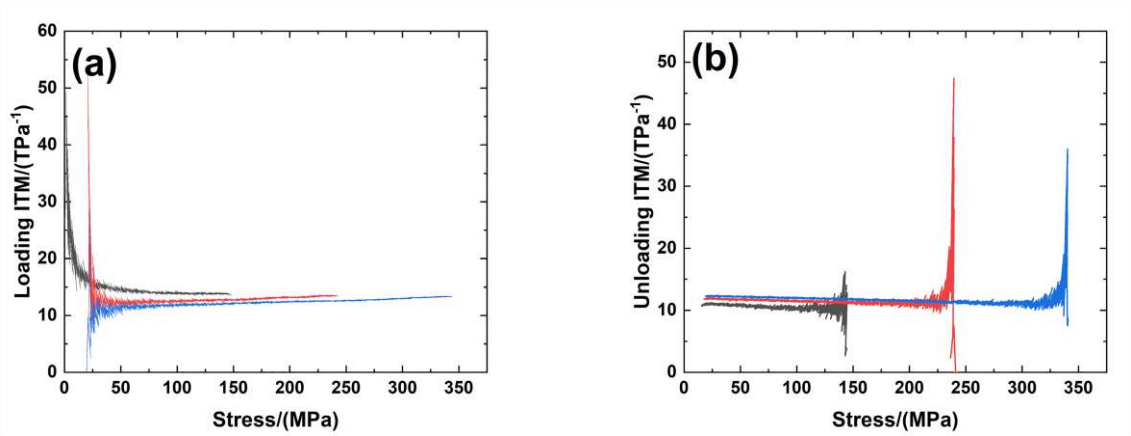

Fig. 8. (a) Loading ITM; and (b) unloading ITM versus applied stress curves of SiC/SiC minicomposite without BNNTs for different peak stresses of σ_{max} = 150, 250, and 350 MPa

4.2 Original and fracture surface observation of SiC/SiC minicomposites with and without BNNTs under SEM

Using ball milling – annealing process, the in situ BNNTs were grown on the surface of SiC fibers. **Fig. 9** shows the microstructure of the surface of SiC fibers with BNNTs under SEM. It can be found that the BNNTs were successfully grown on the surface of SiC fibers, and the grown was compact and evenly covered on the fibers' surface.

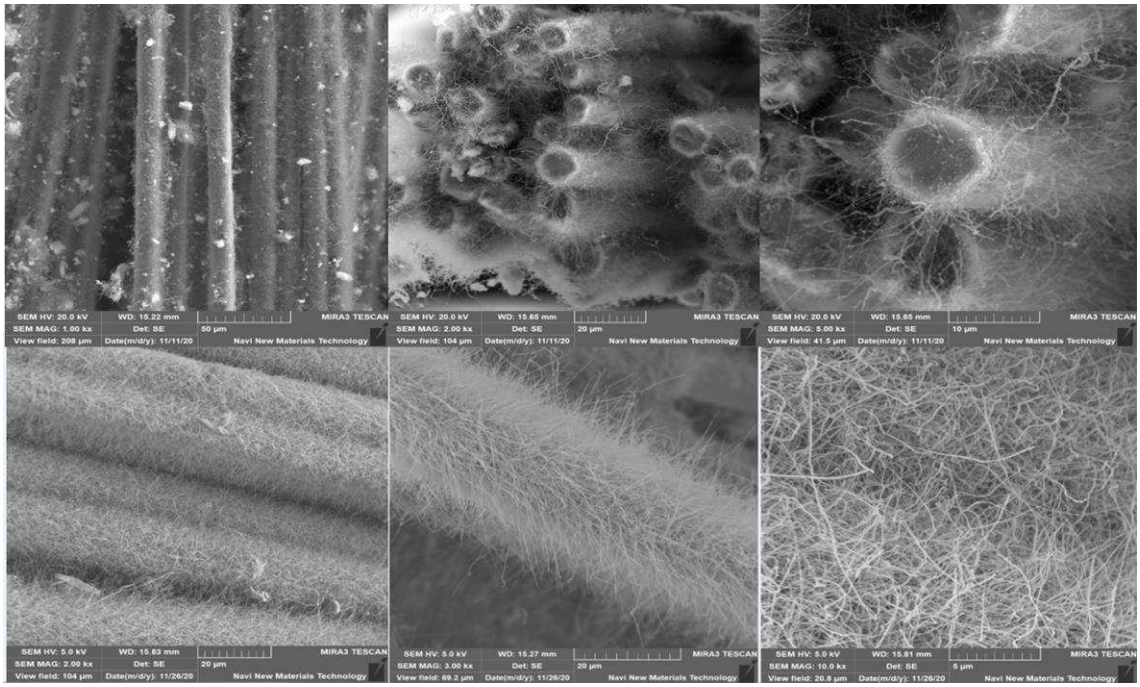

Fig. 9. Microstructure observation on surface of SiC fibers with BNNTs under SEM

The element analysis was performed for the SiC fibers' surface, as shown in **Fig. 10**. It was found that B and N are the main elements on the surface, in addition, a small amount of Fe and Mg also existed. **Table 4** shows the ratio of different elements, including: B, N, Si, C, O, Mg, and Fe.

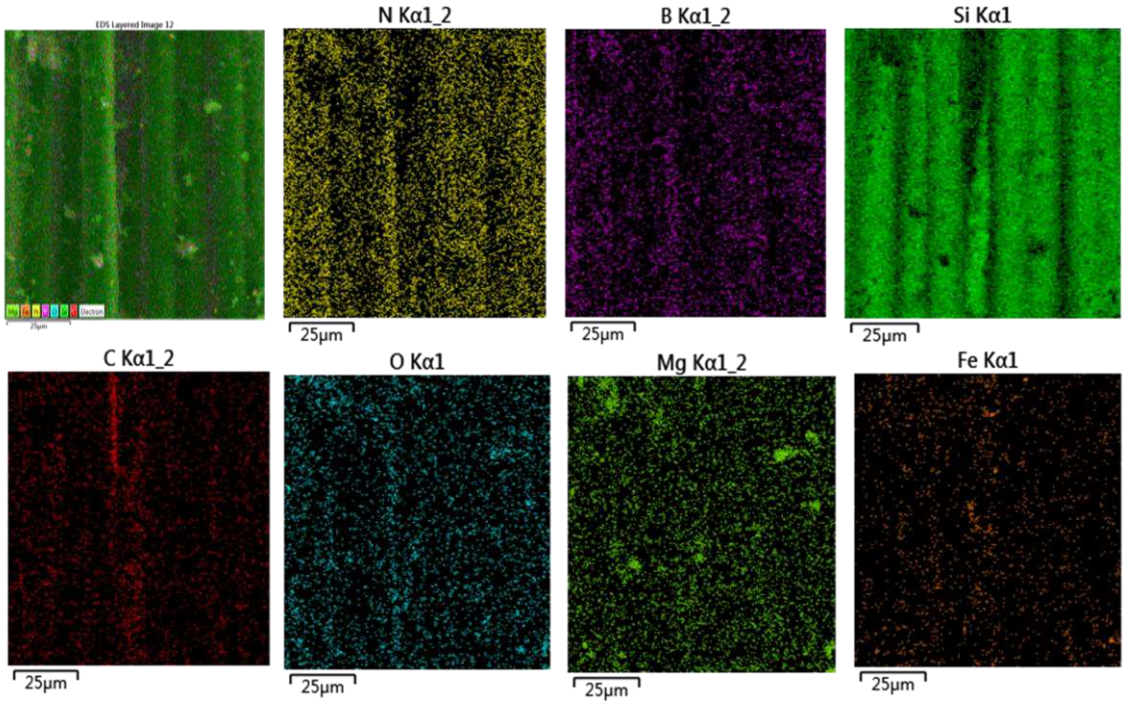

Fig. 10. Element analysis of SiC fiber with BNNTs.

Table 4. Ratio of different elements of SiC fiber with BNNTs

Element	B	N	Si	C	O	Mg	Fe
Weight %	39.1	30.5	12.5	11.5	5.3	0.6	0.5

Fig.s 11 and 12 show the fracture morphology of SiC/SiC minicomposites with and without BNNTs. For SiC/SiC minicomposite with BNNTs, the pullout length of the SiC fiber was short, and the fracture surface was planar. There is no obvious PyC interphase on the SiC fibers' surface. During the annealing at approximately 1300 ^{o}C, the PyC interphase may oxidize with O_2. Without the interphase, the composite exhibited low tensile fracture strength and failure strain. For SiC/SiC minicomposite without BNNTs, the PyC interface existed on the surface of SiC fibers with the thickness of approximately 150 – 200 nm. The interphase plays function of load transfer between the fiber and the matrix and leads to long fiber's pullout length. The mechanical properties of SiC/SiC minicomposite without BNNTs is better than that of SiC/SiC minicomposite with BNNTs. To illustrate the effect of annealing at elevated temperature on composite's mechanical properties, **Fig. 13** shows the fracture morphology of SiC/SiC minicomposite after heat-treatment at 1300 ^{o}C. It can be found that the fracture surface of the composite was planar, and few fiber's pullout appeared.

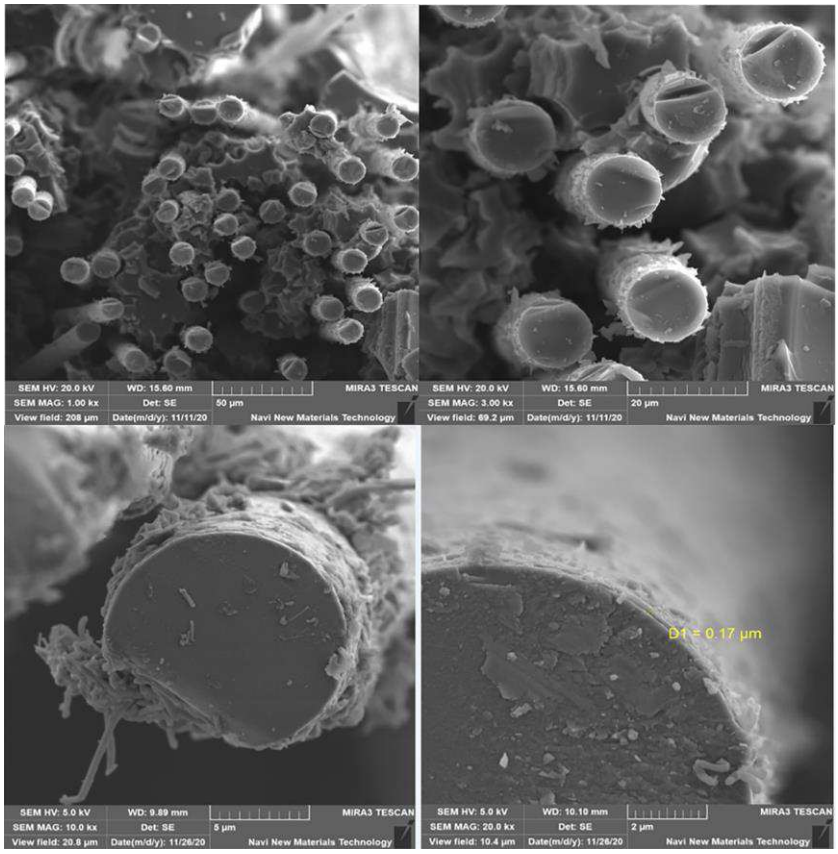

Fig. 11. Fracture morphology of SiC/SiC minicomposite with BNNTs.

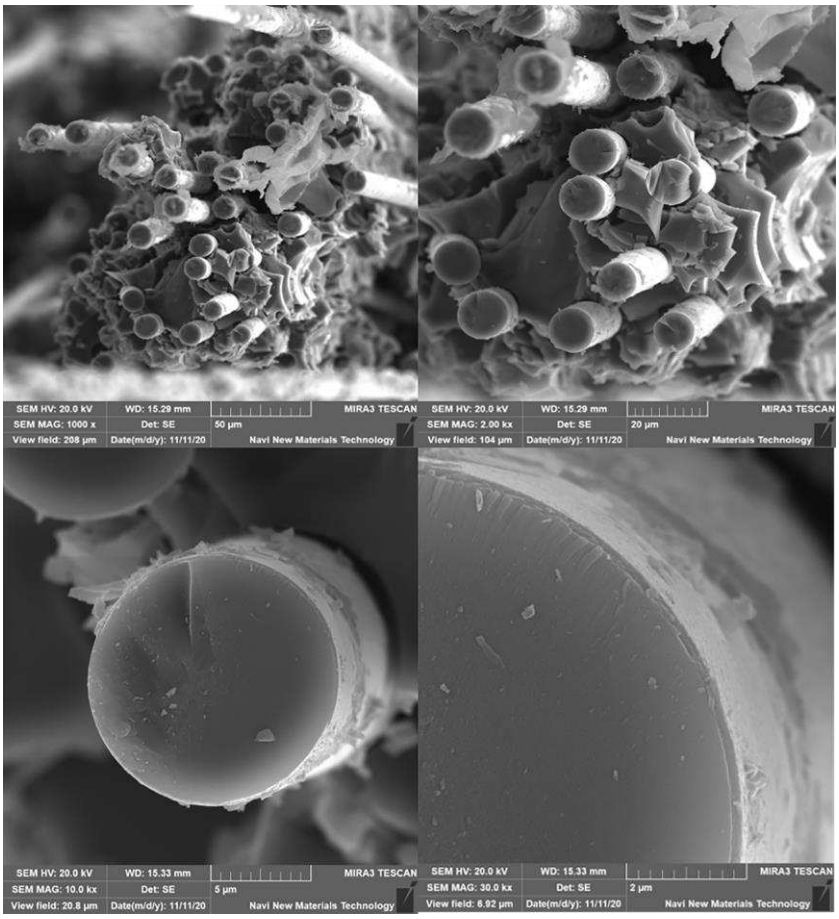

Fig. 12. Fracture morphology of SiC/SiC minicomposite without BNNTs.

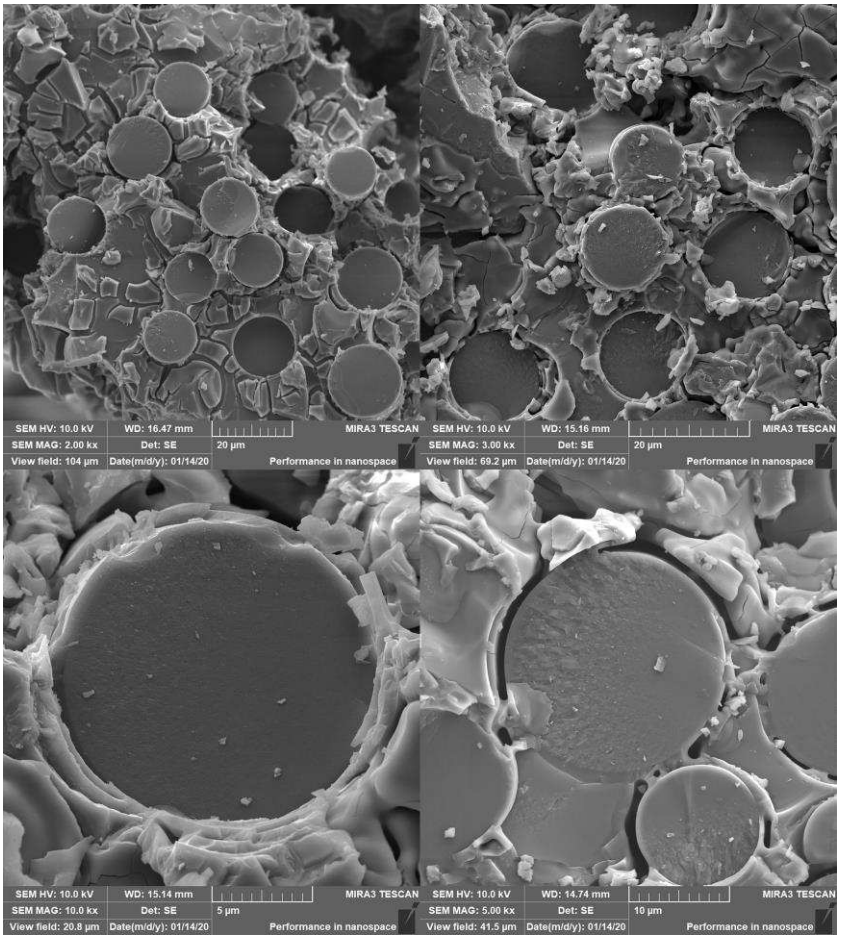

Fig. 13. Fracture morphology of SiC/SiC minicomposite after heat-treatment at 1300 °C.

4.3 Experimental comparisons

Under tensile loading, nonlinear behavior appears for the SiC/SiC minicomposite with and without BNNTs. In the section 3, a micromechanical constitutive relationship is developed considering different damage mechanisms occurred in the composites under tensile loading. The nonlinear stress-strain curves of SiC/SiC minicomposite with and without BNNTs can be predicted using the developed constitutive models. The evolution of broken fiber fraction versus applied strain can also be predicted.

Fig. 14 shows experimental and predicted tensile stress-strain curves and broken fiber fraction versus strain curves of SiC/SiC minicomposite with BNNTs. Considering multiple micro damage mechanisms of matrix fragmentation, interface debonding, and fiber fragmentation, the predicted tensile stress-strain curves agreed with experimental data. Under tensile loading, fibers' failure occurred at applied strain of approximately ε_c = 0.15%; and approached tensile fracture, the broken fiber fraction lied in the range of P = 0.35 – 0.48%.

Fig. 15 shows experimental and predicted composite's tangent modulus versus applied stress curves of SiC/SiC minicomposite with BNNTs. With increasing tensile stress, the composite's tangent modulus decreased from approximately E_P = 82 to 52 GPa.

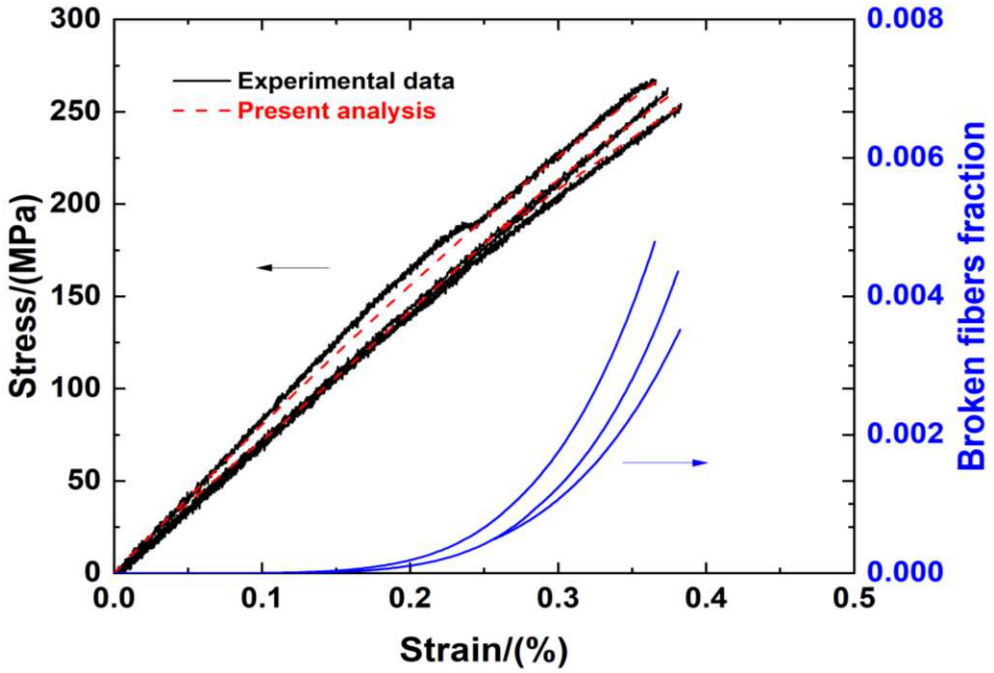

Fig. 14. Experimental and predicted tensile stress-strain curves and broken fiber fraction versus applied strain curves of SiC/SiC minicomposites with BNNTs.

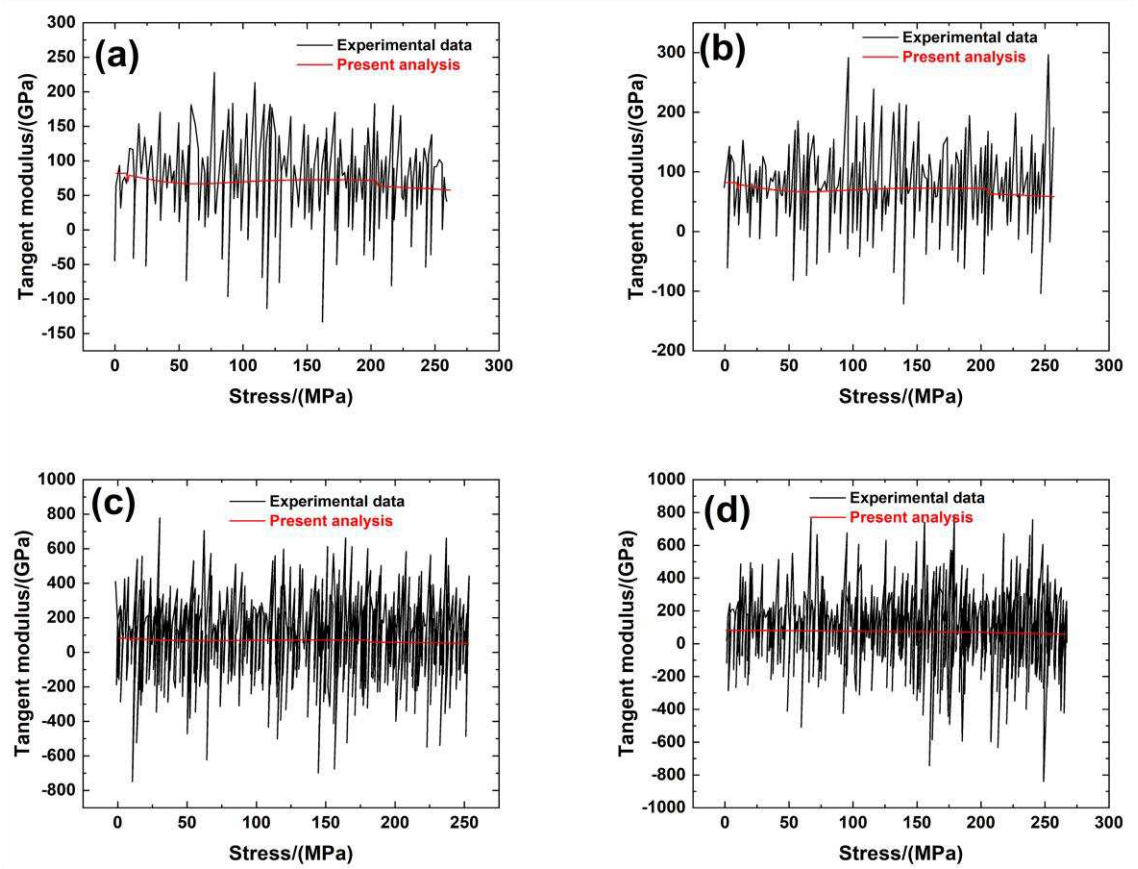

Fig. 15. Experimental and predicted composite's tangent modulus versus applied stress curves of SiC/SiC minicomposite with BNNTs.

Fig. 16 shows experimental and predicted tensile stress-strain curves and broken fiber fraction versus applied strain curves of SiC/SiC minicomposite without BNNTs. Considering multiple damage mechanisms of matrix fragmentation, interface debonding, and fiber fragmentation, the predicted tensile stress-strain curves agreed with experimental data. Under tensile loading, fibers' failure occurred at applied strain of approximately $\varepsilon_c = 0.15\%$, and approached tensile fracture, the broken fiber fraction lied in the range of $P = 1.6 – 2.2\%$.

Fig. 17 shows experimental and predicted composite's tangent modulus versus applied stress curves of SiC/SiC minicomposite without BNNTs. With increasing tensile stress, the composite's tangent modulus decreased from approximately $E_P = 93$ to 50.2 GPa.

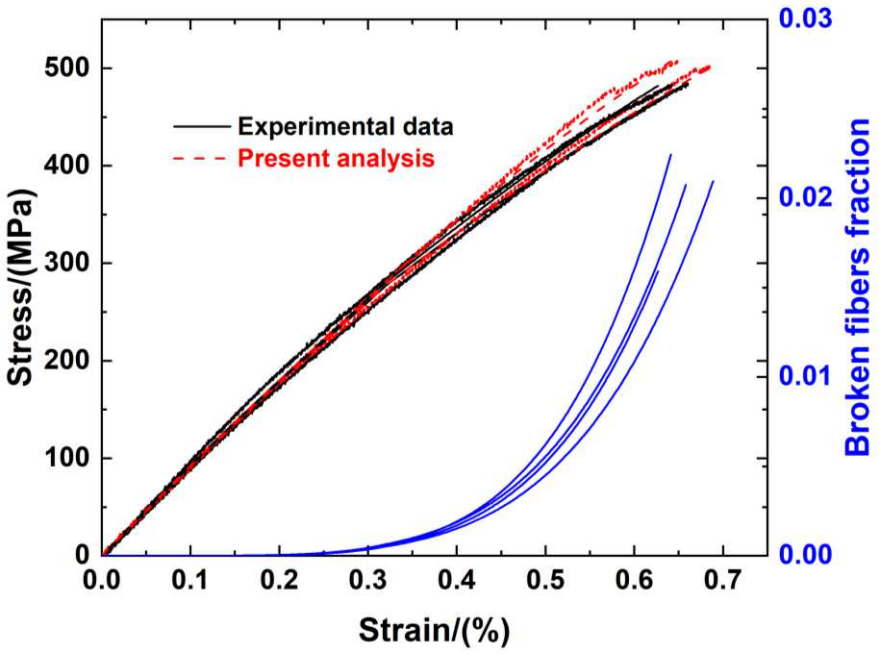

Fig. 16. Experimental and predicted tensile stress-strain curves and broken fiber fraction versus applied strain curves of SiC/SiC minicomposites without BNNTs.

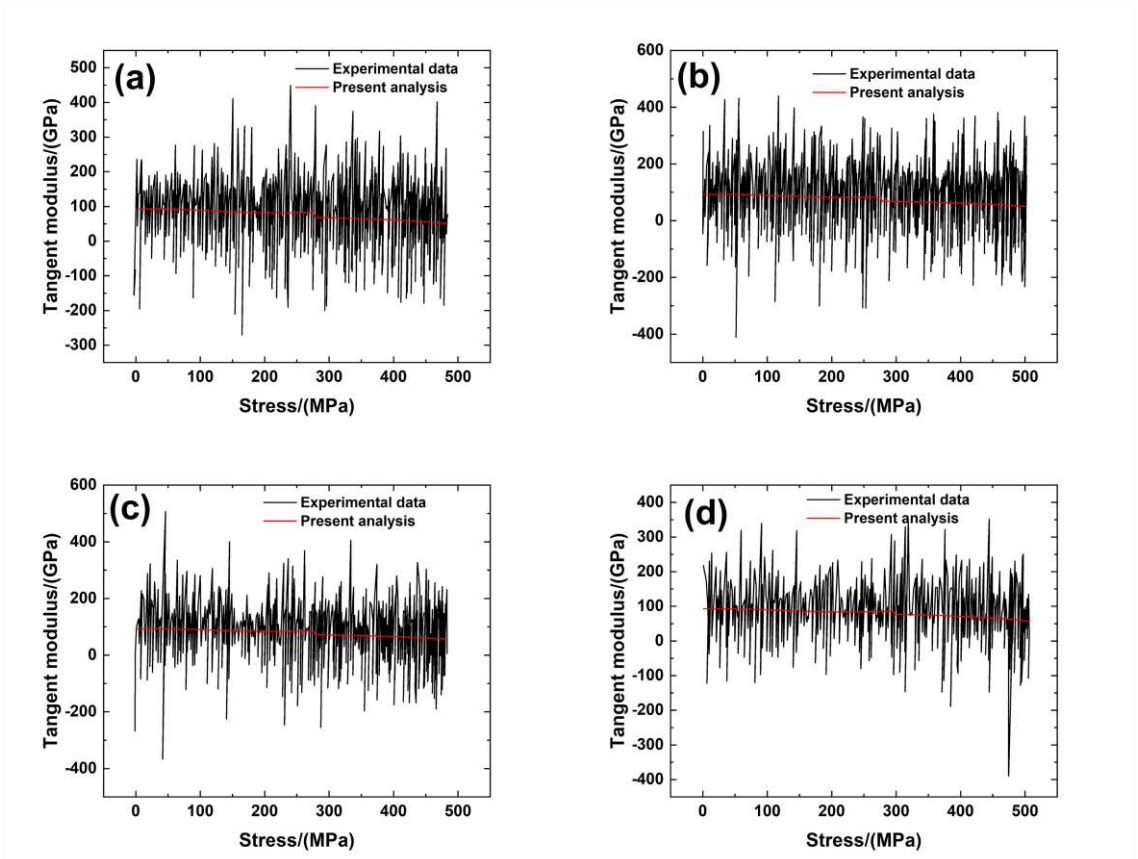

Fig. 17. Experimental and predicted composite's tangent modulus versus applied stress curves of SiC/SiC minicomposite without BNNTs.

5. Conclusions

In this paper, the SiC/SiC minicomposites with and without BNNTs were fabricated by using the PIP method. Effect of in situ grown BNNTs on monotonic tensile and compliance tensile behavior was analyzed. Mechanical properties of composite's elastic modulus, tensile strength, and fracture strain under tensile loading were obtained. Under cyclic compliance tensile, the ITMs for different peak stresses were also analyzed. After tensile fracture, the specimens were observed under SEM to reveal internal damage mechanisms. Experimental tensile stress-strain curves, broken fiber fraction, and composite's tangent modulus were predicted using the developed micromechanical constitutive model.

- Under monotonic tensile loading, for SiC/SiC minicomposite with BNNTs, the average composite tensile elastic modulus was approximately E_c = 74 GPa, the average composite tensile strength was approximately σ_{UTS} = 260.6 MPa, and the composite's fracture strain lied in the range between ε_f = 0.366 and 0.383%; for the SiC/SiC minicomposites without BNNTs, the average composite's tensile elastic modulus was approximately E_c = 92.6 GPa, the average composite tensile strength was approximately σ_{UTS} = 494.7 MPa, and the tensile fracture strain lied in the range between ε_f = 0.642 and 0.683%.
- The SiC/SiC composite without BNNTs were heat-treated at 1300 ^oC. The composite's tensile strength was approximately σ_{UTS} = 163 MPa, and the corresponding fracture strain was approximately ε_f = 0.31%. It can be found that after heat-treatment at 1300 ^oC, the mechanical properties of the SiC/SiC minicomposite degraded rapidly and were less than the values of SiC/SiC minicomposite with BNNTs.
- Under compliance tensile loading, for SiC/SiC minicomposite with and without BNNTs, the loading ITM increased with increasing applied stress and then remained constant. The unloading ITM increased with decreasing applied stress to the constant value.
- At the fracture surface, for SiC/SiC minicomposite with BNNTs, the pullout

length of the SiC fiber was short. There was no obvious PyC interphase on the SiC fibers' surface. For SiC/SiC minicomposite without BNNTs, the PyC interface existed on the surface of SiC fibers with the thickness of approximately 150~200 nm. For the SiC/SiC minicomposite after heat-treatment at 1300 ºC, the fracture surface of the composite was planar, and few fiber's pullout appeared.

Conflict of Interest

The authors declare that they have no known competing financial interests or personal relationships that could have appeared to influence the work reported in this paper.

Acknowledgements

The work reported here is supported by the National Natural Science Foundation of China (Grant No. 51902348, 52002403), Open Research Fund Program of Science and Technology on Aerospace Chemical Power Laboratory (Grand No. STACPL120181b05-2) and the Project (ZZYJKT2020-11) of State Key Laboratory of High Performance Complex Manufacturing, Central South University, and the Fundamental Research Funds for the Central Universities of China (Grant No. NS2019038).

References

[1] Naslain R. Design, Preparation and properties of non-oxide CMCs for application in engines and nuclear reactors: an overview. Compos Sci Technol 2004; 64:155–170. https://doi.org/10.1016/S0266-3538(03)00230-6

[2] Li LB. Damage, fracture and fatigue of ceramic-matrix composites. Springer Nature, Singapore, 2018. https://www.springer.com/in/book/9789811317828

[3] Li LB. Thermomechanical fatigue of ceramic-matrix composites. Wiley-VCH, Weinheim,

Germany. 2019.
https://onlinelibrary.wiley.com/doi/book/10.1002/9783527822614

[4] Li LB. Durability of ceramic matrix composites. Woodhead Publishing, Oxford, UK. 2020.
https://doi.org/10.1016/C2018-0-03346-0

[5] Naslain R, Lamon J, Pailler R, Bourrat X, Guette A, Langlais F. Micro/minicomposites: a useful approach to the design and development of non-oxide CMCs. Compos Part A 1999; 30:537–547.
https://doi.org/10.1016/S1359-835X(98)00147-X

[6] Golberg D, Bando Y, Tang C, Zhi C. Boron nitride nanotubes. Adv Mater 2007; 19:2413–2432.
https://doi.org/10.1002/adma.200700179

[7] Zhi C, Bando Y, Tang C, Golberg D. Boron nitride nanotubes. Mater Sci Eng R 2010; 70:92–111.
https://doi.org/10.1016/j.mser.2010.06.004

[8] Zhi CY, Bando Y, Tang CC, Huang Q, Golberg D. Boron nitride nanotubes: functionalization and composites. J Mater Chem 2008; 18:3900–3908.
https://doi.org/10.1039/B804575E

[9] Bansal NP, hurst JB, Chois R. Boron nitride nanotubes-reinforced glass composites. J Am Ceram Soc 2006; 89:388–390.
https://doi.org/10.1111/j.1551-2916.2005.00701.x

[10] Choi SR, Bansal NP, Garg A. Mechanical and microstructural characterization of boron nitride nanotubes-reinforced SOFC seal glass composite. Mater Sci Eng A 2007; 460:509–515.
https://doi.org/10.1016/j.msea.2007.01.084

[11] Huang Q, Bando YS, Xu X, Nishimura T, Zhi C, Tang C, Xu F, Gao L, Golberg D. Enhancing superplasticity of engineering ceramics by introducing BN nanotubes. Nanotechnology 2007; 18:485706-7.
https://doi.org/10.1088/0957-4484/18/48/485706

[12] Hurst J. Boron nitride nanotubes, silicon carbide nanotunes and carbon nanotubes- a comparison of properties and applications. In: Nanotube Superfiber Materials, Edited by Mark J Schulz, Vesselin N Shanov and Zhangzhang Yin, William Andrew Publishing, 2013.
https://doi.org/10.1016/B978-1-4557-7863-8.00009-8

[13] Li LB, Song Y, Sun Y. Modeling the tensile behavior of unidirectional C/SiC ceramic-matrix composites. Mech Compos Mater 2014; 49:659–672. https://doi.org/10.1007/s11029-013-9382-y

[14] Li LB. Modeling the monotonic and cyclic tensile stress-strain behavior of 2D and 2.5D woven C/SiC ceramic-matrix composites. Mech Compos Mater 2018; 54:165–178. https://doi.org/10.1111/j.1551-2916.2004.01726.x

[15] Li LB. Effect of stochastic loading on tensile damage and fracture of fiber-reinforced ceramic-matrix composites. Materials 2020; 13:2469. https://doi.org/10.3390/ma13112469

[16] Li LB. A time-dependent tensile constitutive model for long-fiber-reinforced unidirectional ceramic-matrix minicomposites considering interface and fiber oxidation. Int J Damage Mech 2020; 29:1138–1166. https://doi.org/10.1177/1056789520924103

[17] Maillet E, Godin N, R'Mili M, Reynaud P, Fantozzi G, Lamon J. Damage monitoring and identification in SiC/SiC minicomposites using combined acousto-ultralics and acoustic emission. Compos Part A 2014; 57:8-15. https://doi.org/10.1016/j.compositesa.2013.10.010

[18] Whitlow T, Jones E, Przybyla C. In-situ damage monitoring of a SiC/SiC ceramic matrix composite using acoustic emission and digital image correlation. Compos Struct 2016; 158:245-251. http://dx.doi.org/10.1016/j.compstruct.2016.09.040

[19] Curtin WA. Multiple matrix cracking in brittle matrix composites. Acta metal mater 1993; 41:1369–1377. https://doi.org/10.1016/0956-7151(93)90246-O

[20] Gao Y, Mai Y, Cotterell B. Fracture of fiber-reinforced materials. J Appl Math Phys 1988; 39: 550–572. https://doi.org/10.1007/BF00948962

[21] Curtin WA. Theory of mechanical properties of ceramic-matrix composites. J Am Ceram Soc 1991; 74:2837–2845. https://doi.org/10.1111/j.1151-2916.1991.tb06852.x

[22] Shi Y, Kessel F, Friess M, Jain N, Tushtev K. Characterization and modeling of tensile properties of continuous fiber reinforced C/C-SiC composite at high temperatures. J Euro Ceram Soc 2021; Online. https://doi.org/10.1016/j.jeurceramsoc.2020.09.043

Table captions

Table 1. General properties of SiC/SiC minicomposites.

Table 2. Monotonic tensile properties of SiC/SiC minicomposites with BNNTs.

Table 3. Monotonic tensile properties of SiC/SiC minicomposites without BNNTs.

Table 4. Ratio of different elements of SiC fiber with BNNTs.

Table 1

Type of sample	Porosity	Density	Fiber volume content	Fiber orientation
SiC/PyC/SiC	≤ 10 %	≤ 2.5 g/cm^3	45 %	Unidirectional
SiC/PyC/BNNTs/SiC	≤ 8 %	≤ 2.6 g/cm^3	45 %	Unidirectional

Table 2

Specimen	Elastic modulus/(GPa)	Tensile strength/(MPa)	Fracture strain/(%)
#1	71	262.8	0.374
#2	70.2	258.3	0.366
#3	71.5	253.5	0.383
#4	83.5	268.1	0.366
Average value	74	260.6	0.372
Standard deviation	5.47	5.4	0.007

Table 3

Specimen	Elastic modulus/(GPa)	Tensile strength/(MPa)	Fracture strain/(%)
#1	90.2	485.6	0.658
#2	92.4	502.6	0.683
#3	95.9	482.9	0.642
#4	92.1	507.8	0.648
Average value	92.6	494.7	0.657
Standard deviation	2	10.7	0.015

Table 4

Element	B	N	Si	C	O	Mg	Fe
Weight %	39.1	30.5	12.5	11.5	5.3	0.6	0.5

Fig. captions

Fig. 1. Schematic of fabrication of BNNTs using ball milling – annealing method.

Fig. 2. Schematic of tensile specimens of SiC/SiC composites with and without BNNTs.

Fig. 3. Schematic of testing machine and tensile specimen.

Fig. 4. Monotonic tensile stress-strain curves of SiC/SiC minicomposites (a) with BNNTs; and (b) without BNNTs.\

Fig. 5. Tensile stress-strain curve of SiC/SiC minicomposite after heat-treatment at 1300 ^{o}C.

Fig. 6. Cyclic compliance tensile curves of SiC/SiC minicomposites (a) with BNNTs; and (b) without BNNTs.

Fig. 7. (a) Loading ITM; and (b) unloading ITM versus applied stress curves of SiC/SiC minicomposite with BNNTs for different peak stresses of 75, 125, and 175 MPa.

Fig. 8. (a) Loading ITM; and (b) unloading ITM versus applied stress curves of SiC/SiC minicomposite without BNNTs for different peak stresses of 150, 250, and 350 MPa.

Fig. 9. Microstructure observation on surface of SiC fibers with BNNTs under SEM

Fig. 10. Element analysis of SiC fiber with BNNTs

Fig. 11. Fracture morphology of SiC/SiC minicomposite with BNNTs.

Fig. 12. Fracture morphology of SiC/SiC minicomposite without BNNTs.

Fig. 13. Fracture morphology of SiC/SiC minicomposite after heat-treatment at 1300 ^{o}C.

Fig. 14. Experimental and predicted tensile stress-strain curves and broken fibers fraction versus applied strain curves of SiC/SiC minicomposites with BNNTs.

Fig. 15. Experimental and predicted composite tangent modulus versus applied stress curves of SiC/SiC minicomposite with BNNTs.

Fig. 16. Experimental and predicted tensile stress-strain curves and broken fibers fraction versus applied strain curves of SiC/SiC minicomposites without BNNTs.

Fig. 17. Experimental and predicted composite tangent modulus versus applied stress curves of SiC/SiC minicomposite without BNNTs.

Figures

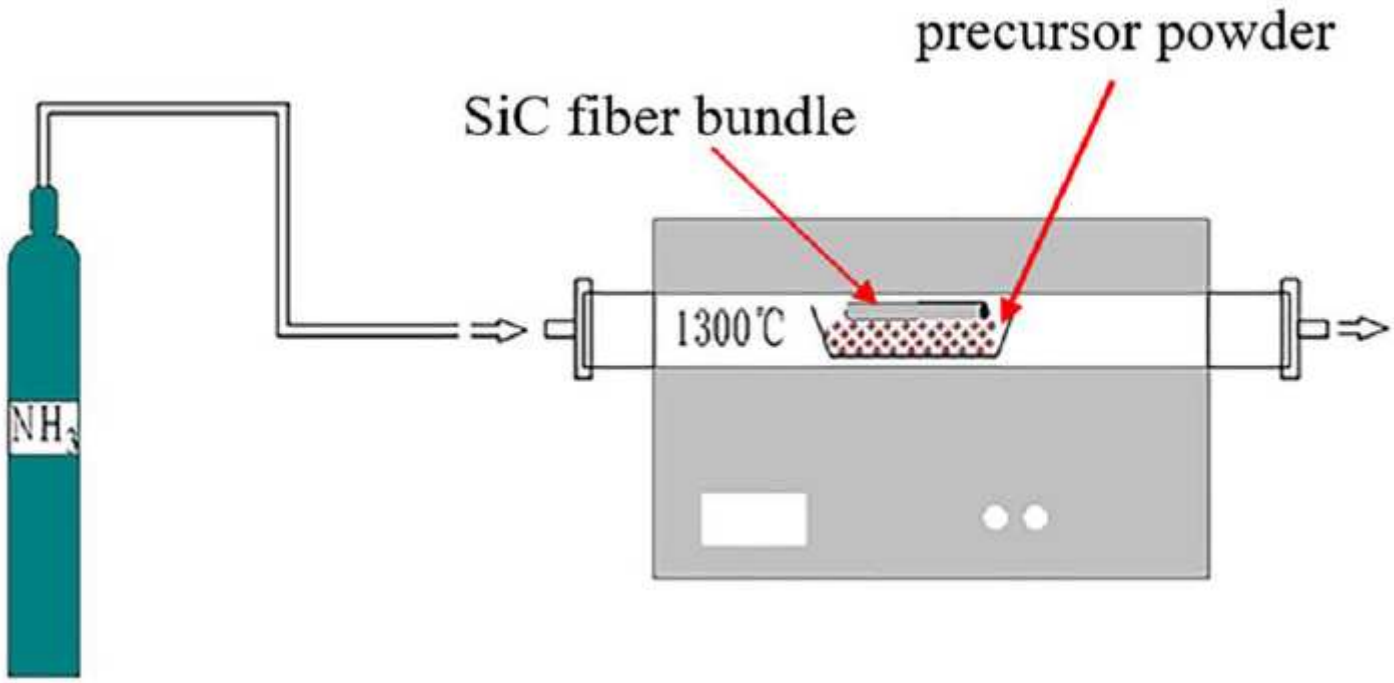

Figure 1

Sc he matic of fabrication of BNN Ts using ball mill ing anneal ing method.

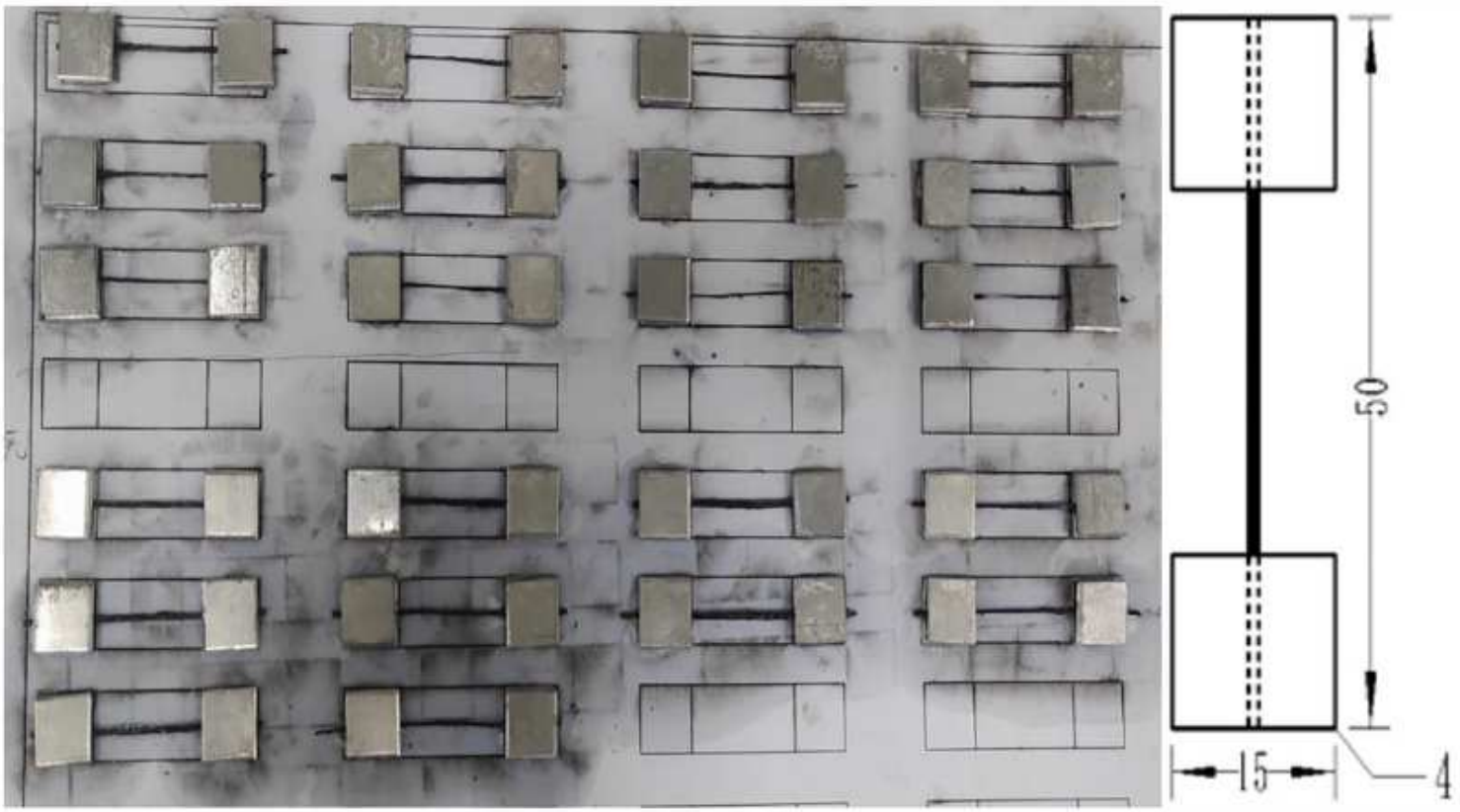

Figure 2

Schematic of tensi le sp e c imens of SiC/S iC co mposites with and without BNNTs.

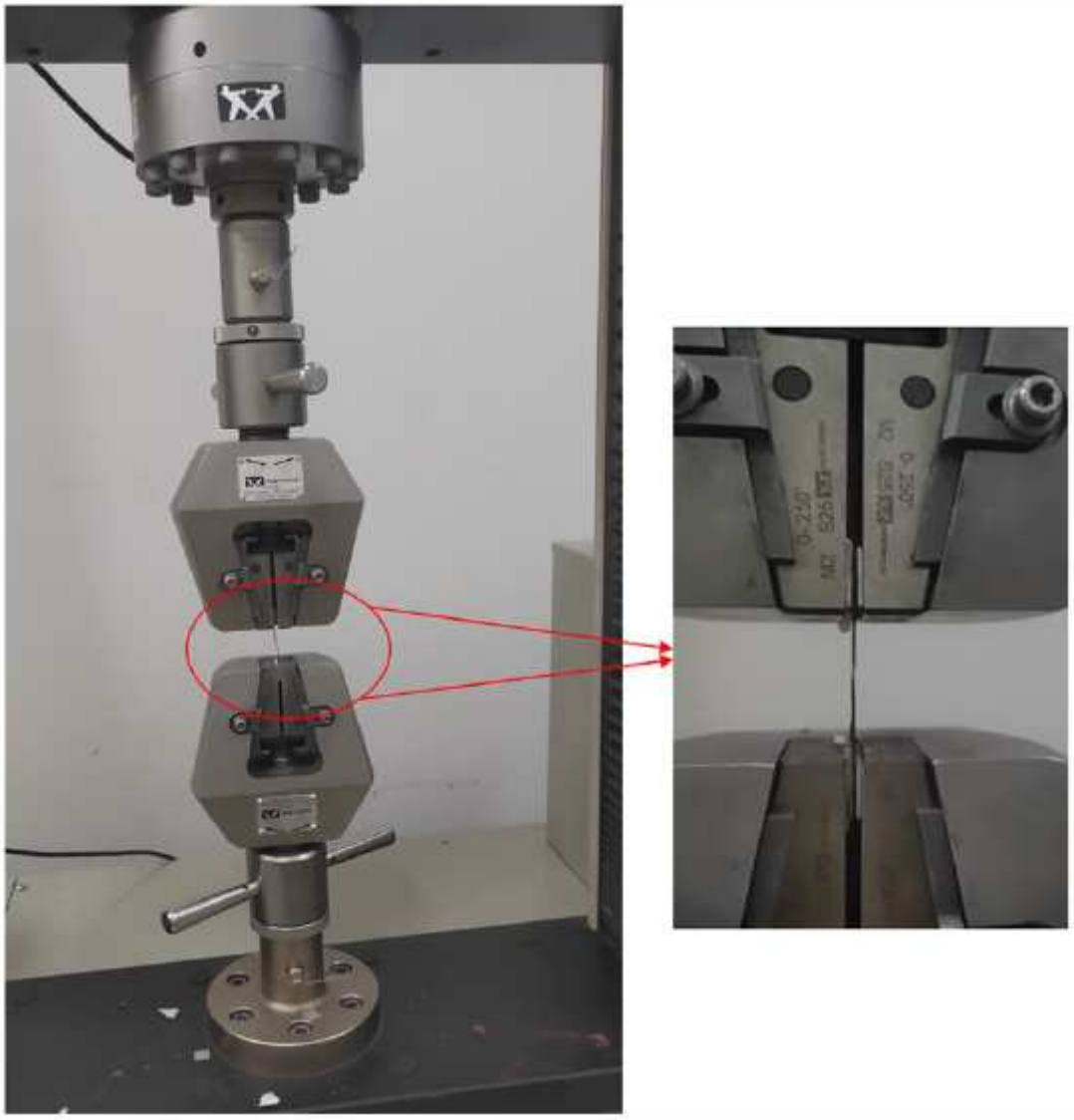

Figure 3

Schematic of testing machine and tensile speci men.

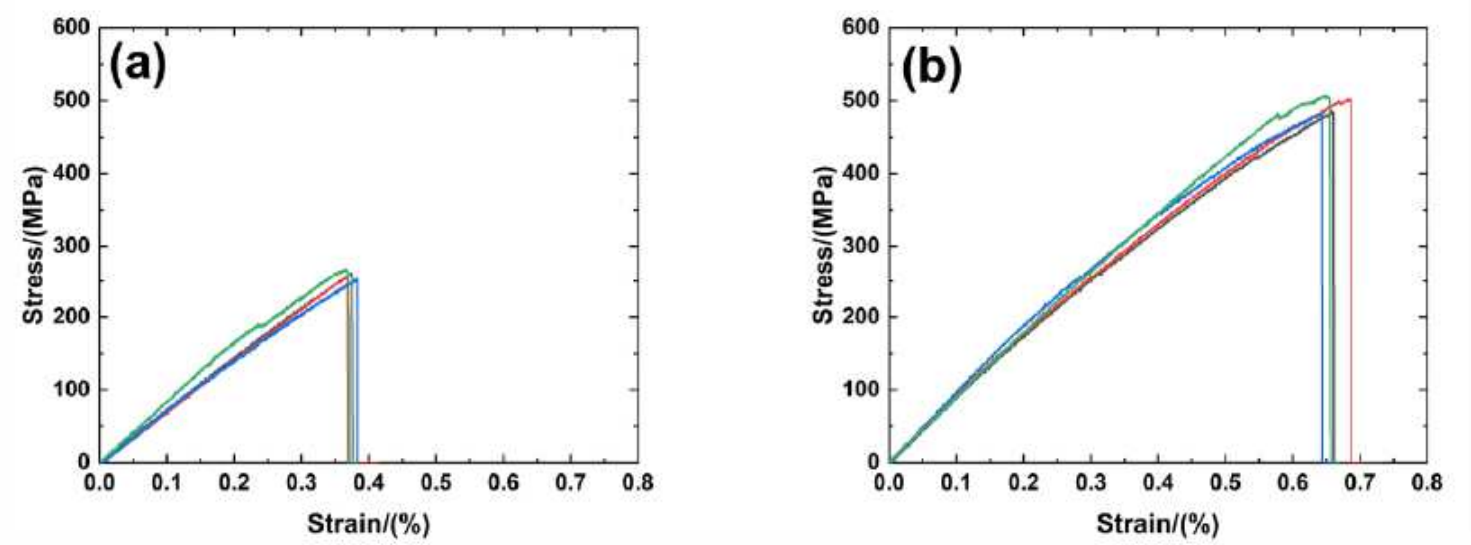

Figure 4

Monotonic tensile stress-strain curves of SiC/SiC minicomposites (a) with BNNTs; and (b) without BNNTs.\

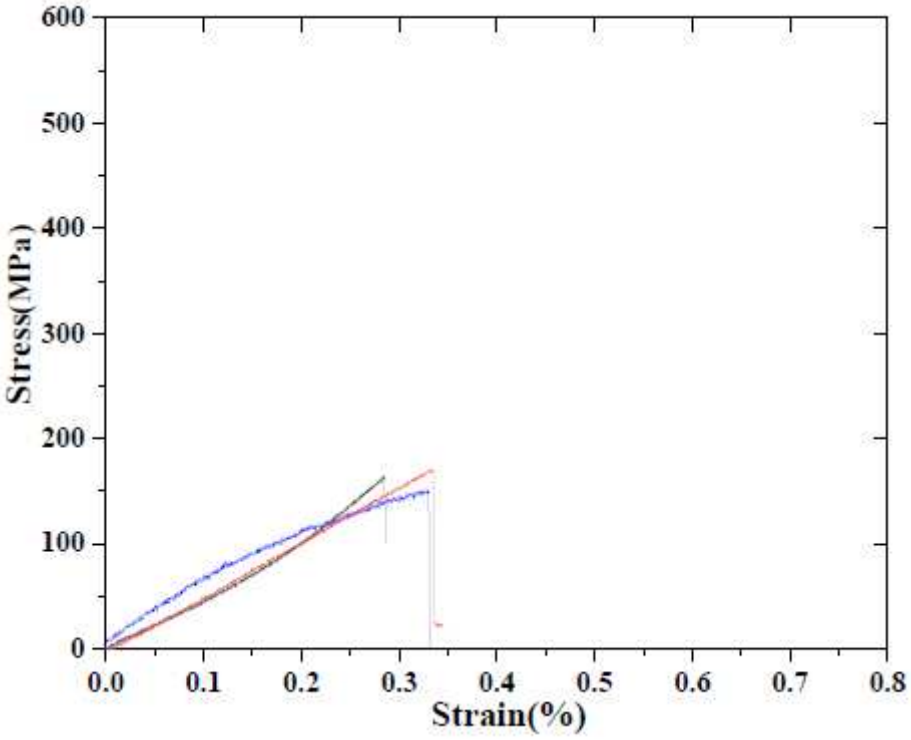

Figure 5

Tensile stress-strain curve of SiC/SiC minicomposite after heat-treatment at 1300 oC.

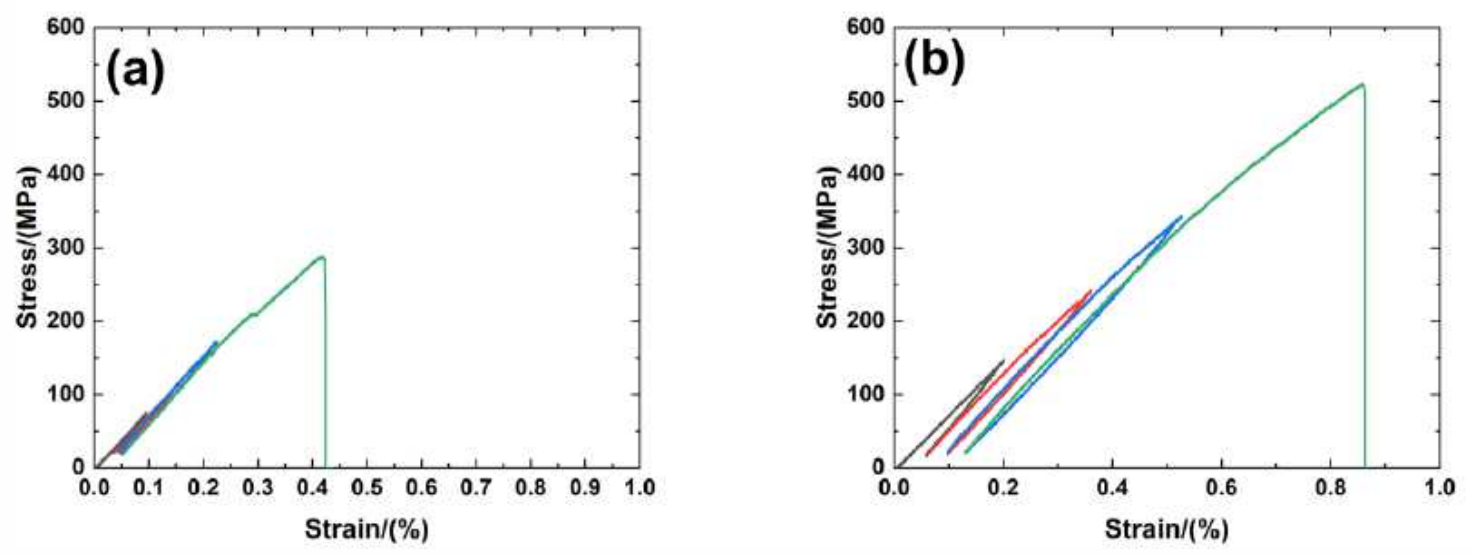

Figure 6

Cyclic compliance tensile curves of SiC/SiC minicomposites (a) with BNNTs; and (b) without BNNTs.

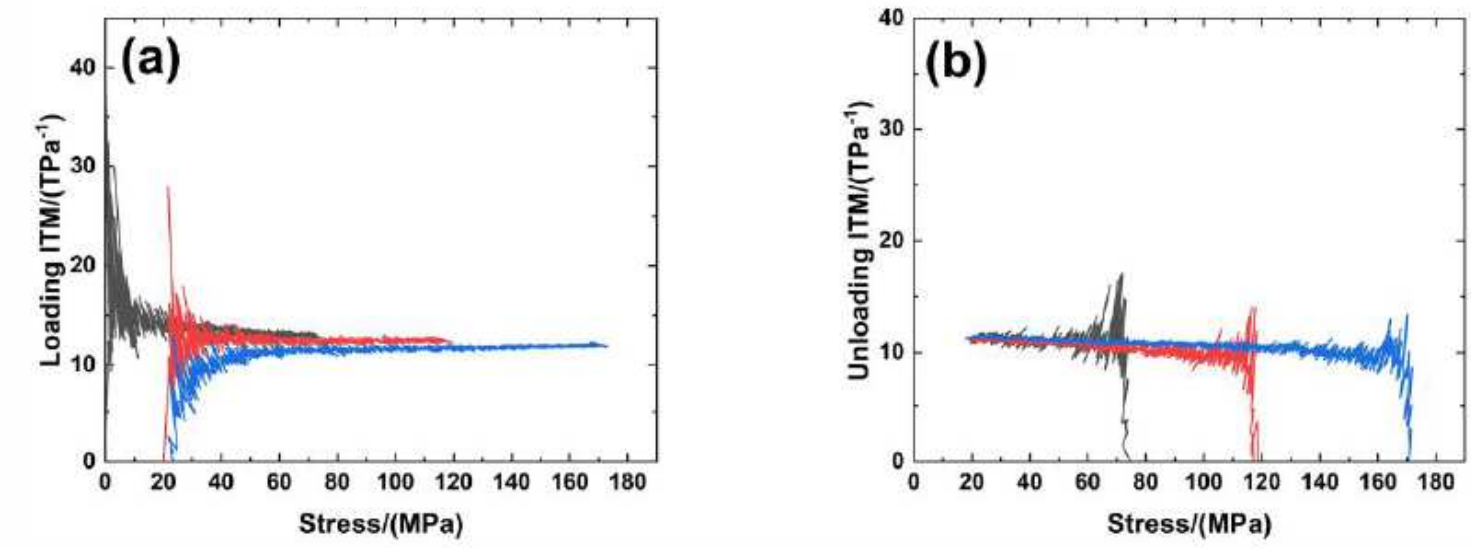

Figure 7

(a) Loading ITM; and (b) unloading ITM versus applied stress curves of SiC/SiC minicomposite with BNNTs for different peak stresses of 75, 125, and 175 MPa.

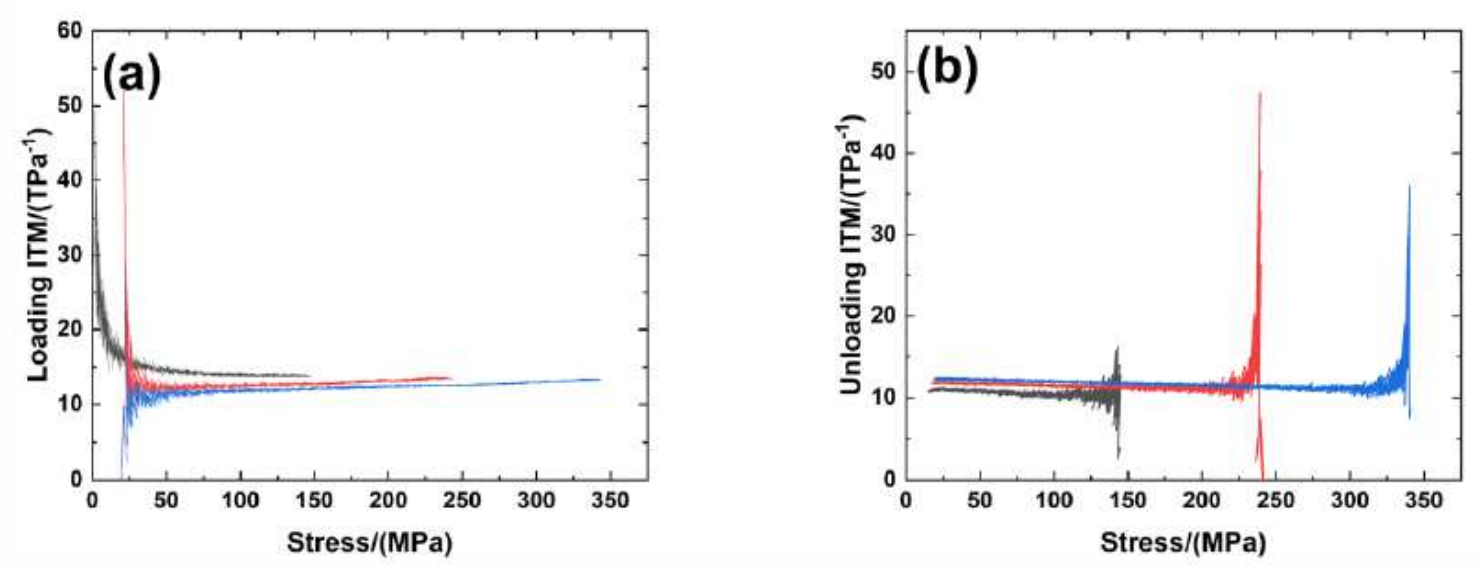

Figure 8

(a) Loading ITM; and (b) unloading ITM versus applied stress curves of SiC/SiC minicomposite without BNNTs for different peak stresses of 150, 250, and 350 MPa.

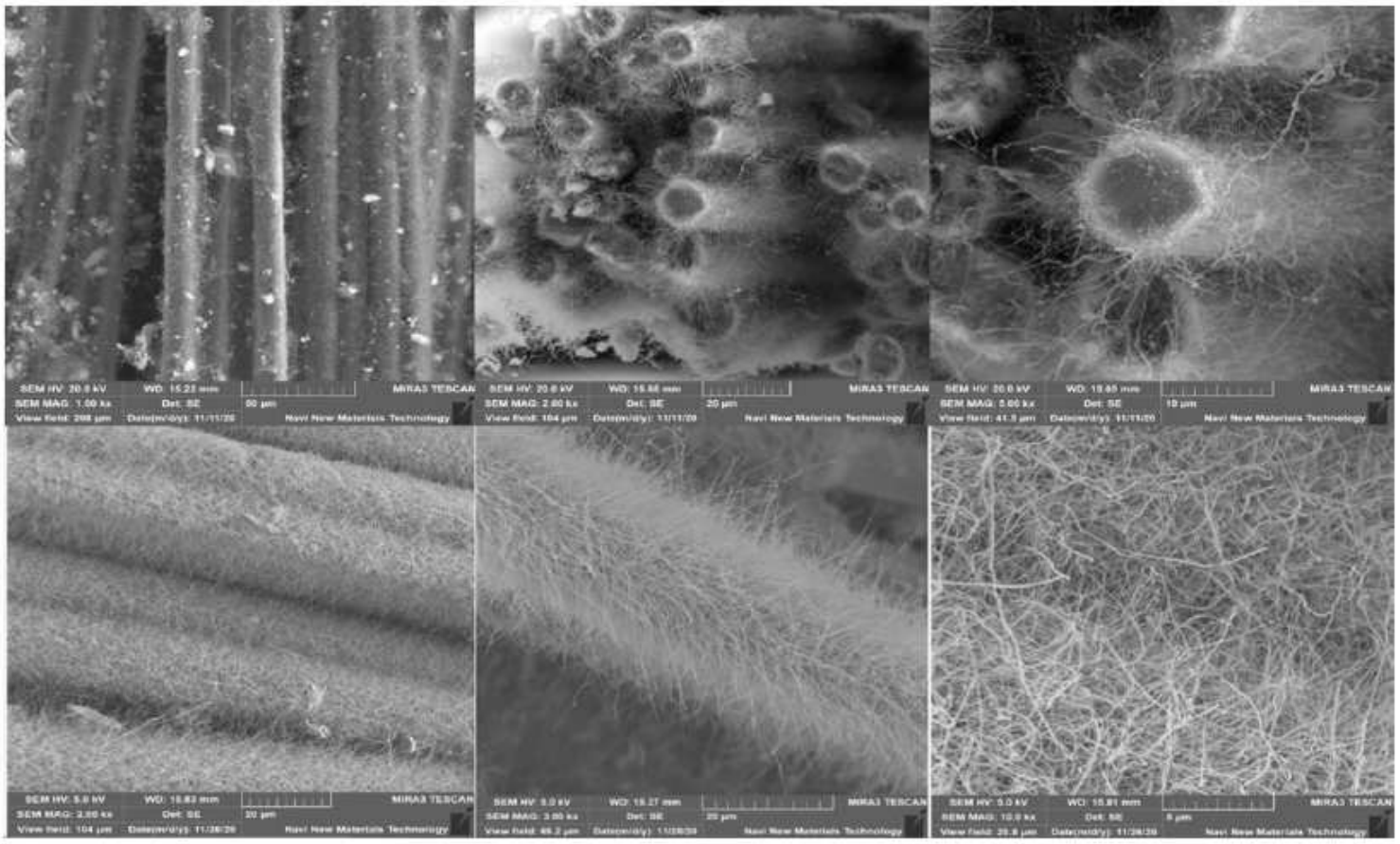

Figure 9

M icrostructure observation on surface of SiC fibers with BN NT s under SEM

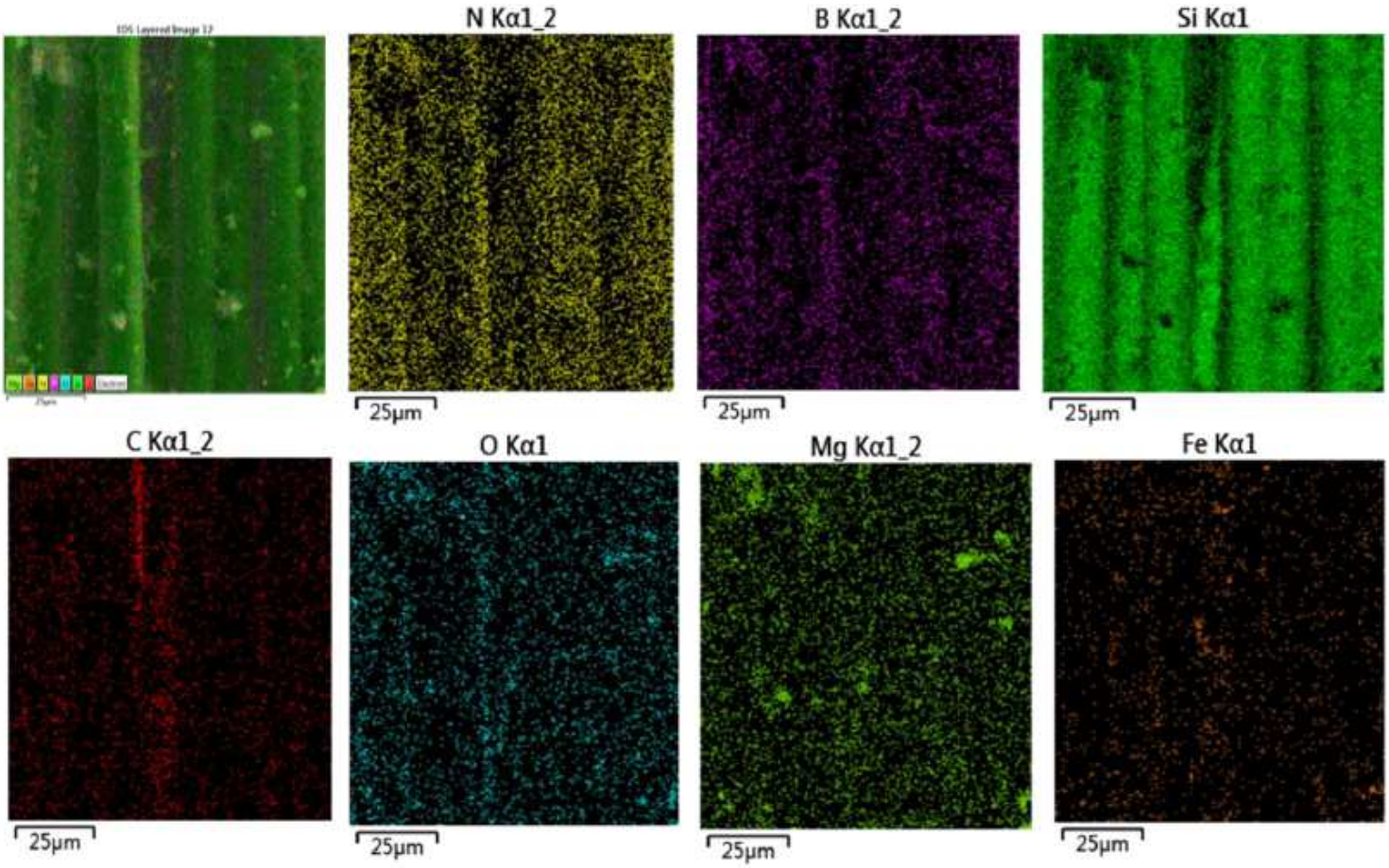

Figure 10

Element analysis of S iC fiber with BNNTs

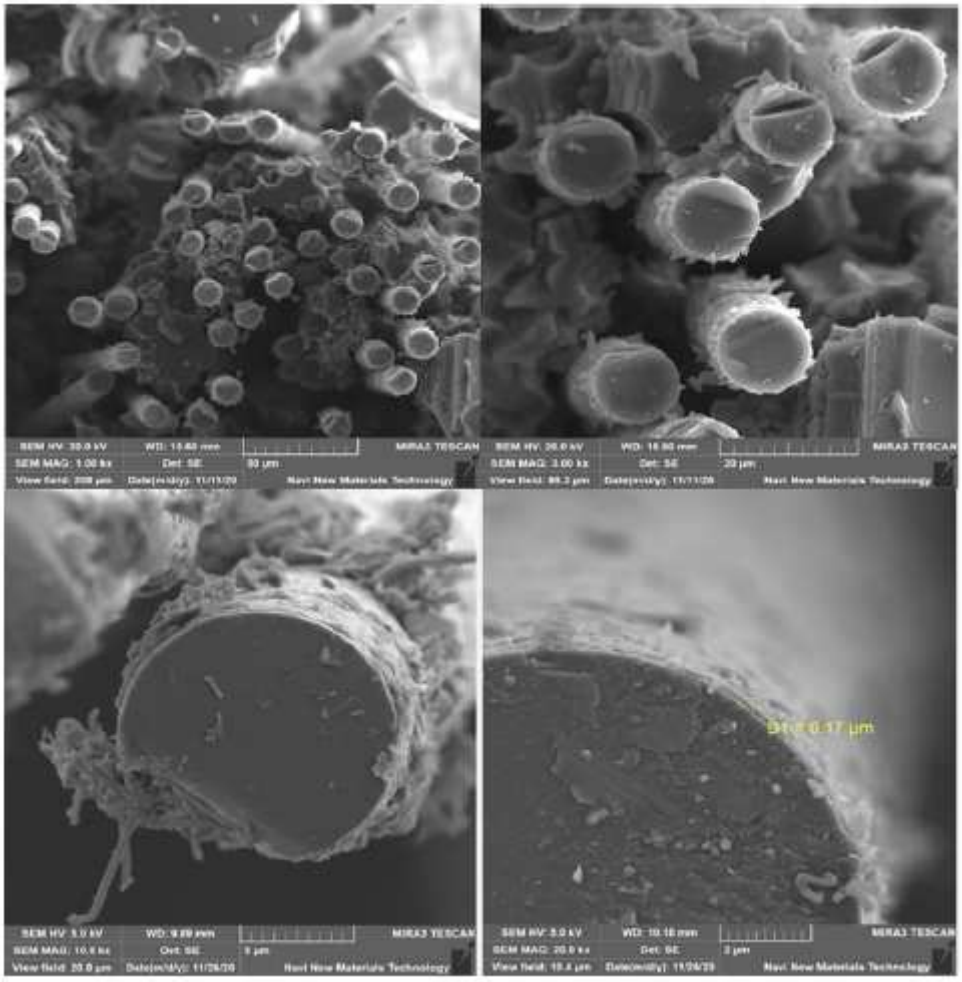

Figure 11

Fracture morphology of SiC/SiC minicomposite with BNNTs.

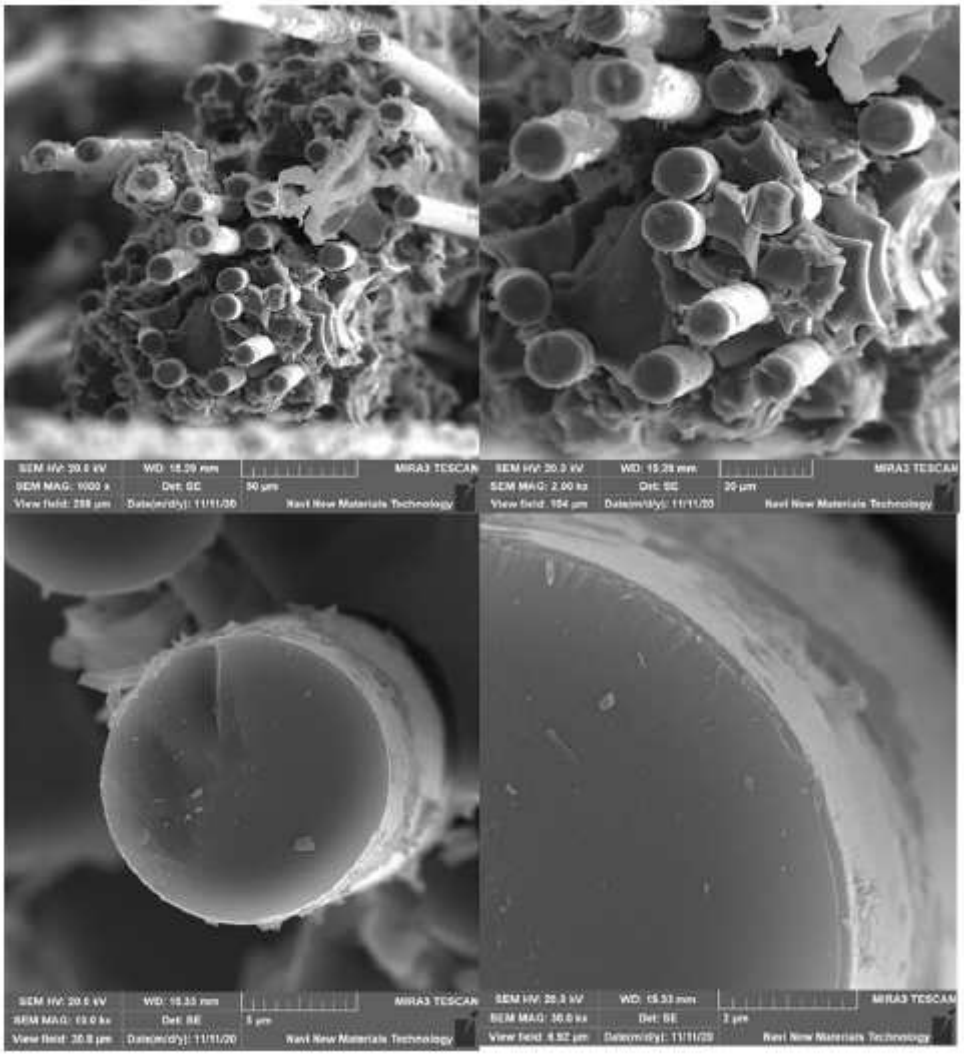

Figure 12

Fracture morphology of SiC/SiC minicomposite without BNNTs.

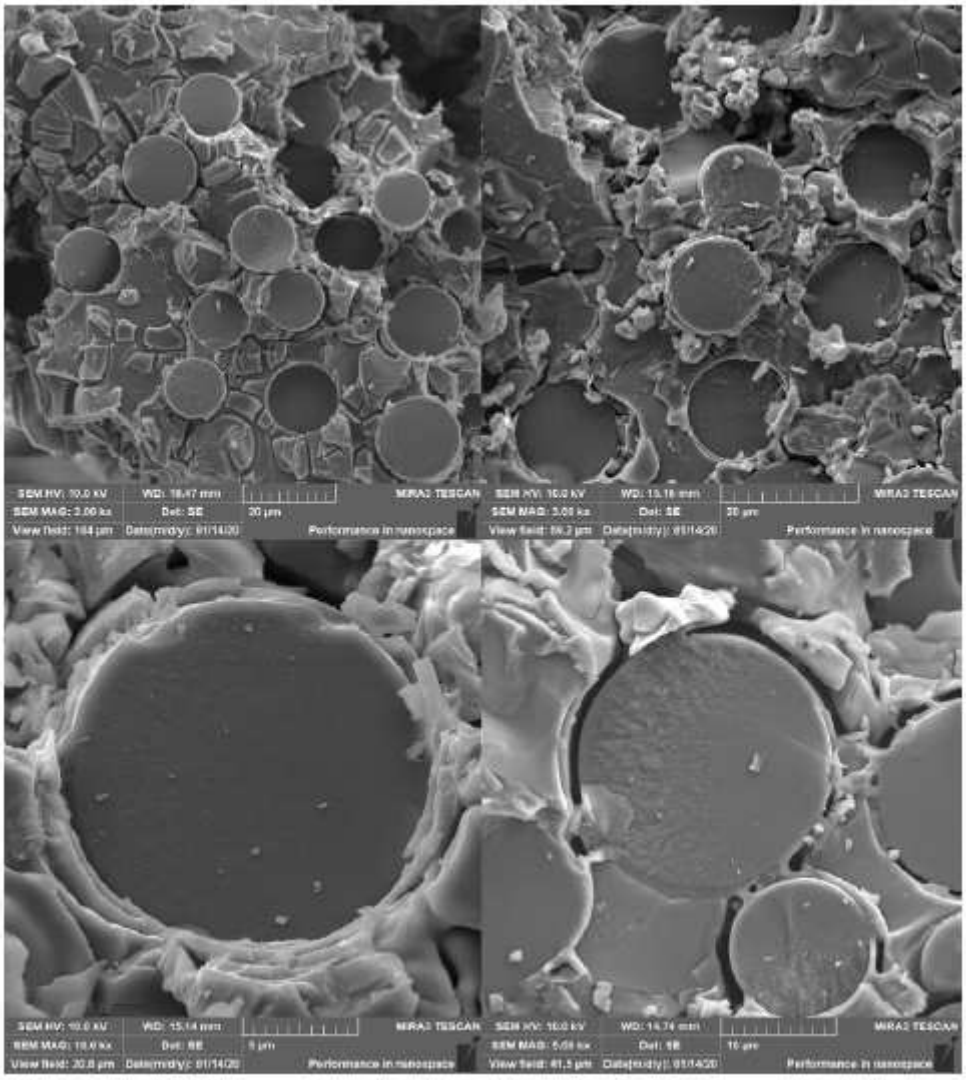

Figure 13

Fracture morphology of SiC/SiC minicomposite after heat-treatment at 1300 oC.

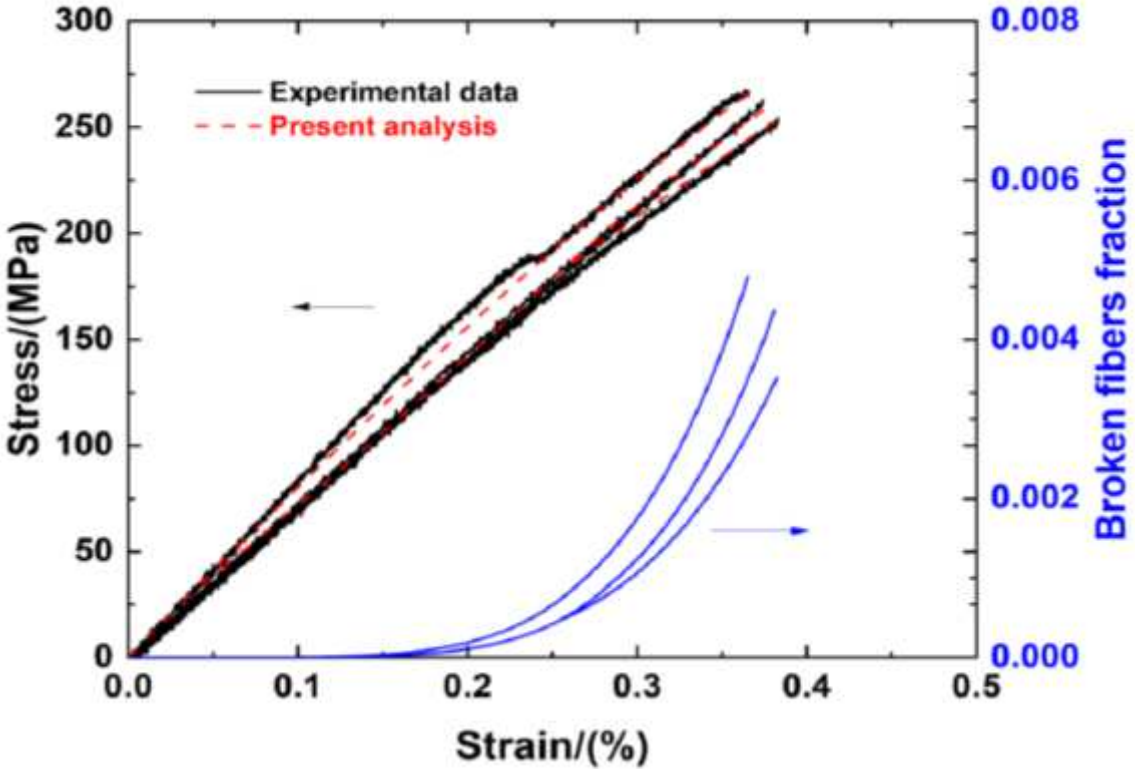

Figure 14

Experimental and predicted tensile stress-strain curves and broken fibers fraction versus applied strain curves of SiC/SiC minicomposites with BNNTs.

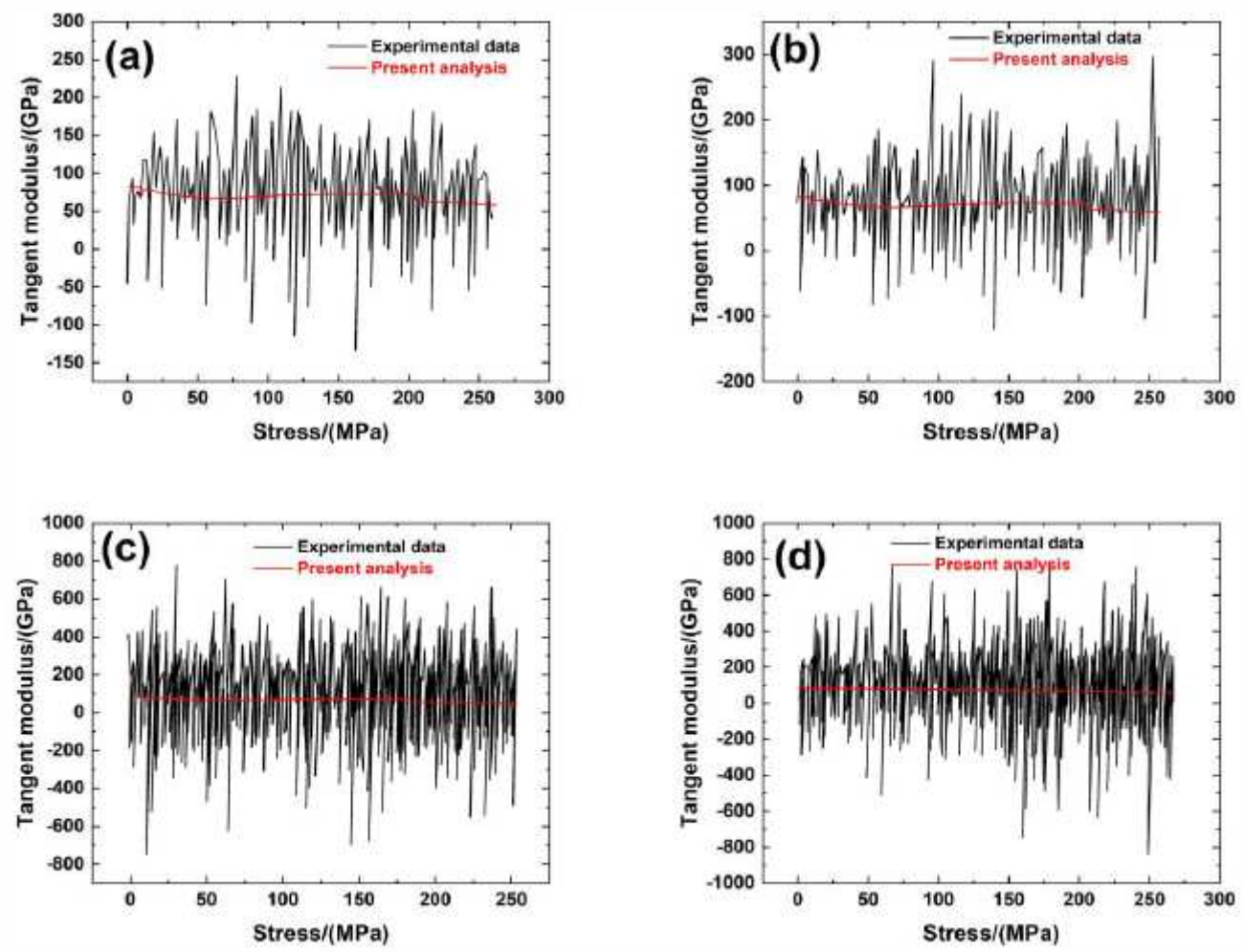

Figure 15

Experimental and predicted composite tangent modulus versus applied stress curves of SiC/SiC minicomposite with BNNTs.

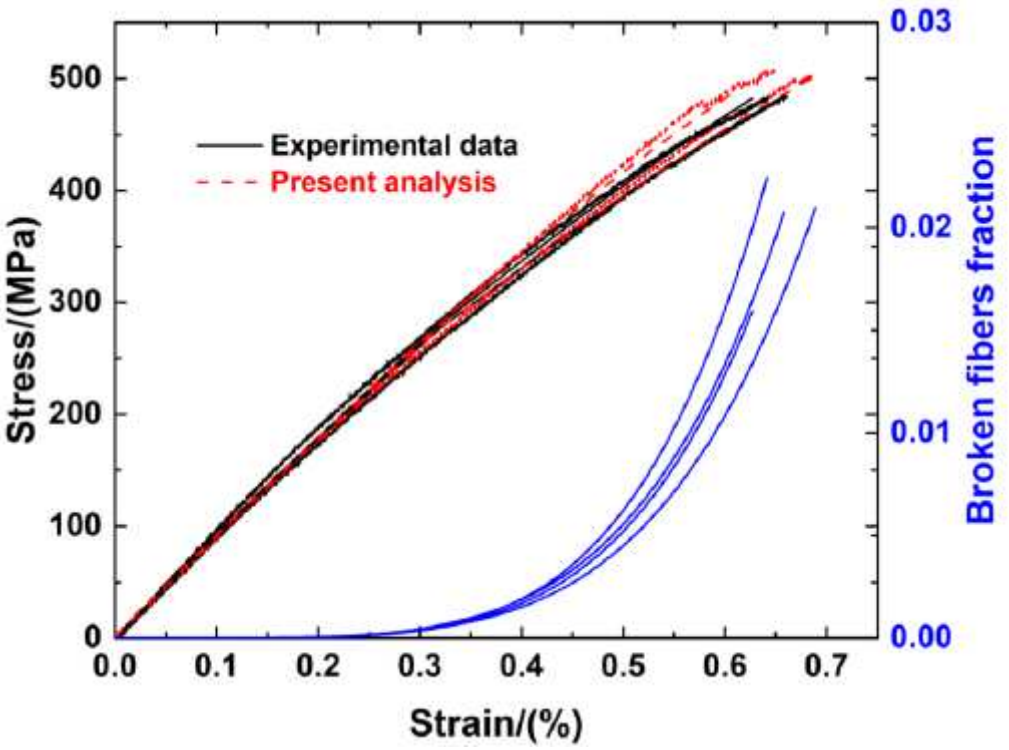

Figure 16

Experimental and predicted tensile stress-strain curves and broken fibers fraction versus applied strain curves of SiC/SiC minicomposites without BNNTs.

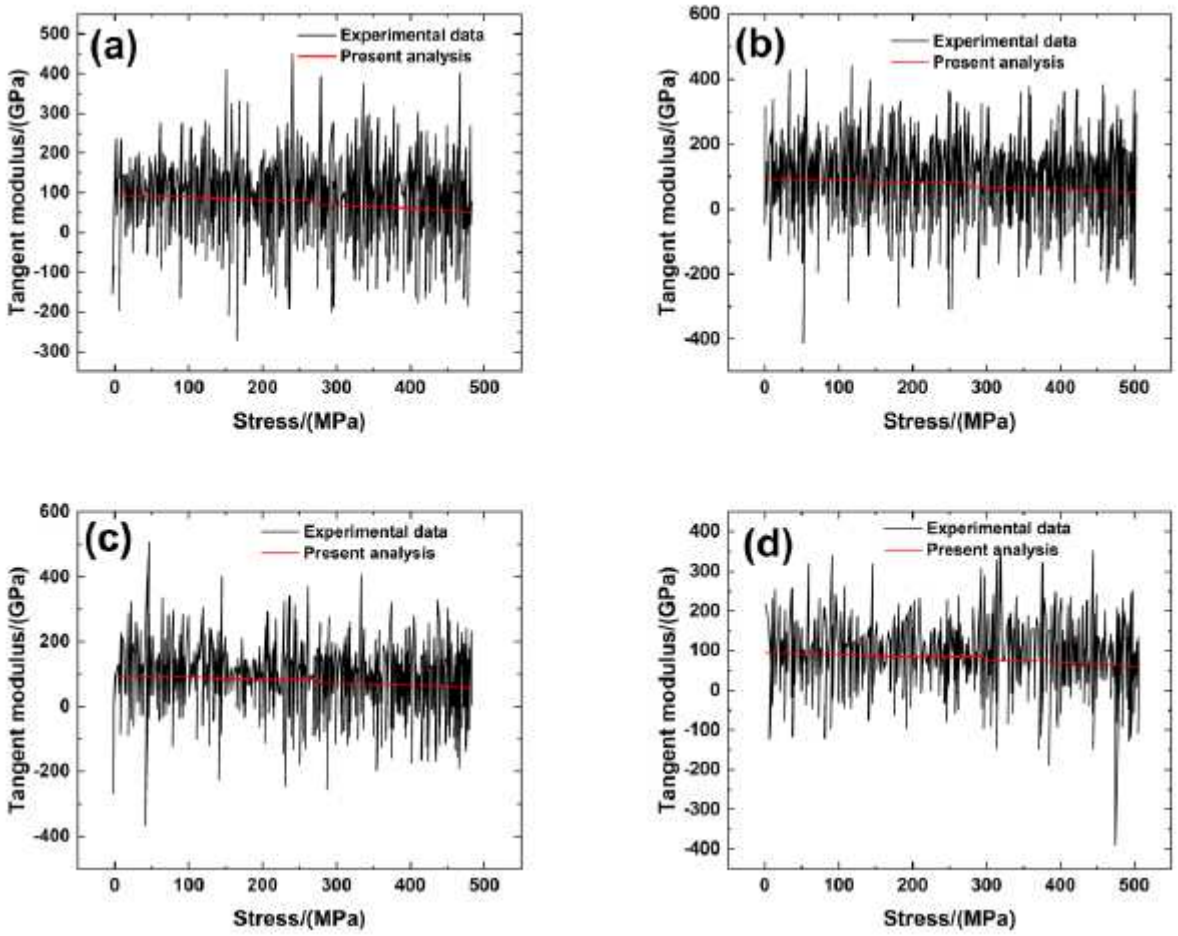

Figure 17

Experimental and predicted composite tangent modulus versus applied stress curves of SiC/SiC minicomposite without BNNTs.